ULTRA-CLEAN TRANSPORTATION FUELS FROM COAL: AN OVERVIEW

John Shen and Edward Schmetz, U.S. Department of Energy, Germantown, MD 20874

Gary J Stiegel, John C Winslow and Robert M Kornosky, National Energy Technology Lab, U.S. Department of Energy, Pittsburgh, PA 15236

Suresh C Jain, National Energy Technology Lab, U.S. Department of Energy, Morgantown WV 26507

Introduction

A recent paper by EIA (Energy Information Administration) within the U.S. Department of Energy (DOE) indicates that coal-to-liquids (CTL) fuels, under the High B Case, could become a viable domestic source to supplement the petroleum liquids supply by 2010[1]. Ultra-clean fuels can be produced from coal via indirect coal liquefaction route. In this technology, coal is first gasified to form synthesis gas (carbon monoxide and hydrogen) which is cleaned to remove impurities and then converted to clean liquid fuels by use of a catalyst using a technology known as Fischer-Tropsch (F-T) synthesis. This paper will review the status of activities supported by the Office of Fossil Energy with DOE which are to help ushering in the early commercial production of CTL fuels.

CTL fuels production via indirect liquefaction is known to be capital sensitive, with syngas production accounting for two thirds of the cost. DOE has been supporting activities aimed to reduce the capital cost of this technology, including the developments of coal gasifier with higher efficiency, advanced syngas cleanup, and slurry-phase F-T synthesis. Significant advances have been made in all areas. A scoping economics study indicates CTL fuels based on these advanced technologies could be competitive with petroleum crude in the mid-$30 per barrel.

A hurdle for the commercial production of CTL fuels is the need to demonstrate the feasibility of the advanced CTL technologies operated in integrated system mode at commercial-scale units to include gasifier, gas cleanup, F-T synthesis, and power generation blocks. This feasibility demonstration has been the focus of two DOE initiatives: (a) Early Entrance Coproduction Plant (EECP), and (b) Clean Coal Power Initiative (CCPI). More specifically, these initiatives aim to produce CTL fuels along with power, chemicals, and steam in a mode called coproduction. Under this mode, a F-T synthesis step would be incorporated into an integrated gasification and combined cycle (IGCC) complex to help achieve higher plant efficiency and a more versatile product slate. This coproduction (poly-generation) mode is deemed to offer the earliest opportunity for the commercial production of CTL fuels in the U.S.

CTL Fuels Projects at the Waste Management Processors, Inc. (WMPI)

Two separate cost-sharing CTL projects were awarded to the WMPI by DOE, the first one under the EECP initiative and the second one under the CCPI initiative. The former is for the project definition and preliminary engineering design, and the latter for the detailed design, construction, and operation of the CTL demonstration plant. Work for both projects has been closely coordinated to ensure the smooth interactions between them. A brief project description is provided below.

Prime contractor: WMPI
Subcontractors: Shell Global Solutions, Uhde GmbH, Sasol Synfuels International, and Nexant, Inc.
Location: Gilberton, Pennsylvania
Feedstock: anthracite coal waste (culm) at 1.4 million tons per year
Products: 5,000 barrels per day of ultracleanfuels[TM], 131 Mw (92 Mw for internal use and 39 Mw for export) of electricity, sulfur, and steam.
Key process blocks: Shell gasification complex, Sasol and ChevronTexaco F-T synthesis and product workup units, and combined cycle plant.
Roles of other subcontractors: Uhde Gmbh will serve as a general engineering contractor for EPC (engineering, procurement, and construction). Nexant Inc. will serve as an engineering consultant.

In March 2005, WMPI received the air permit approval from the Commonwealth of Pennsylvania for the project. Efforts have been continuing to prepare the EIS (environmental impact statement) to comply with the NEPA (National Environmental Policy Act) and to seek product off take agreements. More detailed data on the project can be found elsewhere [2].

EECP CTL Project with the Texaco Energy Systems LLC

The EECP CTL project with the Texaco Energy Systems LLC was carried out in two phases. Phase I work (project definition and conceptual plant design) was completed in December 2000 and Phase II (research, development and testing) in June 2003. The plant design feedstock is petroleum coke rather than coal since the plant will be located at a site adjacent to a host refinery. This feedstock choice offers the advantages of (a) a lower feedstock cost, and (b) a lower capital cost by sharing the existing infrastructures at the host refinery site. A brief project description is provided below.

Prime contractor: Texaco Energy systems LLC
Subcontractors: General Electric (GE), Praxair, and Kellogg Brown and Root (KBR).
Location: Motiva refinery, Port Arthur, Texas
Feedstock: Petroleum coke at 1,235 short tons per day
Products: 457 barrels per day of wax, 125 barrels per day of F-T diesel, 35 barrels per day of F-T naphtha, 55 Mw power for export, sulfur, and steam.
Key process blocks: Texaco gasification complex, Rentech F-T synthesis unit, Bechtel Hy-Finishing[SM] F-T product workup unit, and combined cycle plant.
Roles of other subcontractors: GE (gas turbine testing), Praxair (air separation technology), and KBR (facility engineering integration).

Highlights of the work included:
1. A conceptual F-T EECP plant design was completed which included a financial analysis of internal rate of return for various cases.
2. Confirmed the F-T reactor design basis which is to process a syngas from an advanced gasifier with hydrogen to carbon monixide ratio of 0.67.
3. Proposed a two-stage F-T wax/catalyst separation system which could yield a clean wax with 10 ppm solids content.
4. Identified integration of F-T synthesis with front-end gasification by feeding the F-T water and F-T spent catalysts into the gasifier

5. Confirmed the feasibility to combust low-Btu tail gas (75 Btu/standard cubic feet) from various sources in the plant in a commercial GE gas turbine.

Upon completion of the Phase II, Texaco decided not to proceed with Phase III work (preliminary engineering design) of the EECP project. This decision was partly due to the need to search for a new host refinery site for the project. The Motiva refinery site, which was chosen in the EECP project design study, became unavailable because of the merger between Chevron and Texaco. More detailed data for this project can be found elsewhere [3, 4].

CTL versus GTL Fuels

CTL plants would generally use iron catalyst in the F-T synthesis to take advantage of its intrinsic water-gas-shift activity and higher tolerance of trace impurities. Both attributes are considered beneficial for processing coal-based syngas from advanced gasifiers with low hydrogen to carbon monoxide ratio and containing trace impurities. This catalyst choice is different from the cobalt catalyst used in the gas-to-liquids (GTL) fuels production with a hydrogen-rich syngas. Despite the slight differences in chemical compositions because of the catalyst choice, CTL and GTL diesel have been shown to exhibit similar emission reduction benefits in engine combustion testing[5].

Conclusions

Prospects of higher crude price that began in 2004 are expected to rekindle interests in alternatives to conventional crude oil. The near commercial-readiness of IGCC plants to produce clean power from coal, coupled with the ability to coproduce clean CTL fuels in the same plant, offers the potential for improved energy security. The CTL demonstration projects at WMPI and Texaco, which are co-funded by DOE, are aimed to demonstrate the integrated system operations of advanced CTL technologies at commercial-scale units. In the ongoing WMPI projects, efforts have been underway to seek arrangements for product off take. CTL and GTL diesel fuels have similar attributes and have been shown to exhibit similar emission reduction benefits in engine combustion testing.

References
(1) Caruso, G.F., "Welcome and Opening Remarks", paper presented at the 13th Annual EIA Midterm Outlook and Modeling Conference, April 12, 2005, Washington, DC.
(2) Quarterly technical progress report (July to September 2004) submitted by WMPI PTY, LLC. under DOE Cooperative Agreement DE-FC26-00NT40693, November 2004
(3) Early Entrance Coproduction Plant, Phase I Preliminary Concept Report, submitted by Texaco Energy Systems Inc. under DOE Cooperative Agreement DE-FC26-99FT40658, May 2001
(4) Early Entrance Coproduction Plant, Phase II Final Report, submitted by Texaco Energy Systems LLC under DOE Cooperative Agreement DE-FC26-99FT40658, January 2004

EXSTOL: EXELUS SYNTHESIS GAS-TO-LIQUIDS TECHNOLOGY

Mitrajit Mukherjee, Sankaran Sundaresan

Exelus Inc., 99 Dorsa Avenue, Livingston, NJ 07039

Introduction

The Fischer-Tropsch (FT) Synthesis reaction converts synthesis gas (a mixture of CO and Hydrogen) into liquid hydrocarbons according to[1]:

$$CO + 2 H_2 \rightarrow \text{"–}CH_2\text{–"} + H_2O \qquad \Delta H = -170 \text{ kJ/mol}$$

where "–CH_2-" represents a product consisting mainly of paraffinic hydrocarbons of variable chain length. Because of the enormous exothermicity of the FT synthesis reaction, a very large heat transfer area is required. This is why a large number of 2nd generation FT technologies use slurry bubble columns as the reactor of choice. A principal advantage of slurry bubble column reactors (BCR) over fixed bed reactors is that the presence of a circulating/agitated slurry phase greatly increases the heat transfer rate to cooling surfaces built into the reactor[2]. Further, the small particle size minimizes the negative impact of diffusional resistances within the interior of the catalyst. However, conventional slurry bubble column reactors have several drawbacks[3]:

1. Liquid-phase back-mixing, which is a strong function of reactor diameter, results in a much lower kinetic driving force, requiring a larger reactor volume than a fixed-bed reactor operating at the same conversion.

2. Catalyst/liquid separation can be a significant technical hurdle, which limits minimum catalyst particle size and can be negatively impacted by catalyst particle attrition

3. Hydrodynamics of slurry bubble-column reactors is complex – scale-up issues can pose significant problems.

This paper summarizes the development of a break-through FT technology that has the ability to significantly improve the economics of the process using a multi-functional catalytic system. The cost reduction potential using this next-generation FT technology provides a very strong springboard for overall Gas-to-Liquids (GTL) process viability.

Exelus' Approach

Researchers at Exelus are developing a first-of-a-kind catalytic system for multi-phase reactions that blurs the line of distinction between the reactor and catalyst by incorporating many features one associates with a reactor within the catalyst body. The new catalyst system called the HyperCat, marries all the benefits of slurry operation (low pore-diffusion barriers, high heat and mass-transfer rates, low pressure drop) with the benefits of fixed-bed operation (no filtration issues, plug-flow behavior and easy scale-up) in one system. It is able to do so by achieving better control of the "micro-environment" at the catalyst surface through intensification of heat and mass-transport processes within the reactor. The high level of control allows ideal reaction conditions to prevail at the active sites, enhancing catalyst performance leading to significantly higher activity. As a result, reactor productivity is significantly enhanced – catalyst volume can now be reduced by 50% or more over a conventional slurry bubble column reactor. The higher levels of inter-phase heat and mass-transfer allow the use of steam-coils (low cost item) to be used for removing reaction heat instead of expensive shell-and-tube reactor designs. This will result in a significant reduction in the cost of the Fischer-Tropsch reactor leading to a corresponding decrease in the cost of a GTL complex.

Results & Discussion

Gas Hold-Up. Gas hold-up is a critical parameter in characterizing the hydrodynamic behavior and hence the performance of a bubble column reactor. It determines: a) the reaction rate by controlling the gas-phase residence time and b) the mass-transfer rate by governing the gas-liquid interfacial area. It is mainly a function of the gas velocity and the liquid physical properties. The gas hold-up of the HyperCat system was studied using an air-water system. The gas superficial velocities were varied from 0.1-1.0 m/s. The results are shown in **Figure 1**. The HyperCat gas hold-up is slightly lower than that in a conventional bubble column reactor (~ 30% reduction) and comparable to that in a slurry bubble column with 30-35% solids concentration.[4]
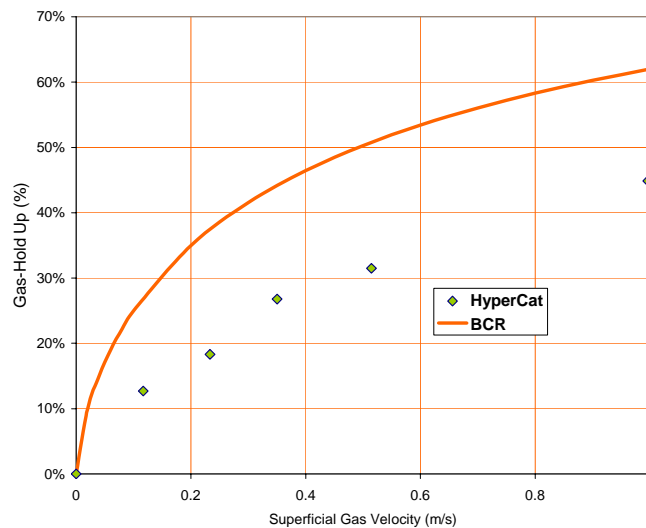

Figure 1. Gas hold-up – HyperCat versus empty bubble column

Liquid-Phase Axial Dispersion. The liquid phase axial dispersion in bubble column reactors is very high making them effectively back-mixed reactors for industrial scale systems. Liquid mixing in bubble columns is a result of global convective re-circulation of the liquid phase and turbulent diffusion due to eddies generated by the rising bubbles. Turbulent diffusion arises from motion on many scales and reflects both large-scale fluctuations caused by the large-scale eddies, and small-scale fluctuations arising from the entrainment of liquid in the wakes of the fast-rising bubbles[5]. By structuring the gas and the liquid flow, HyperCat reduces the axial dispersion for both phases leading to a large reduction in axial dispersion coefficients (D_{AX}). The real benefit of this reduced dispersion is that it is not a function of the reactor diameter as is the case with conventional bubble column reactors.

We measured the liquid phase D_{AX} for a range of gas velocities shown in **Figure 2**. The dispersion values measured for the HyperCat are roughly 2 orders of magnitude lower than those found in commercial scale reactors – which means that the HyperCat reactor will behave like a plug-flow reactor for both the liquid and gas-phases
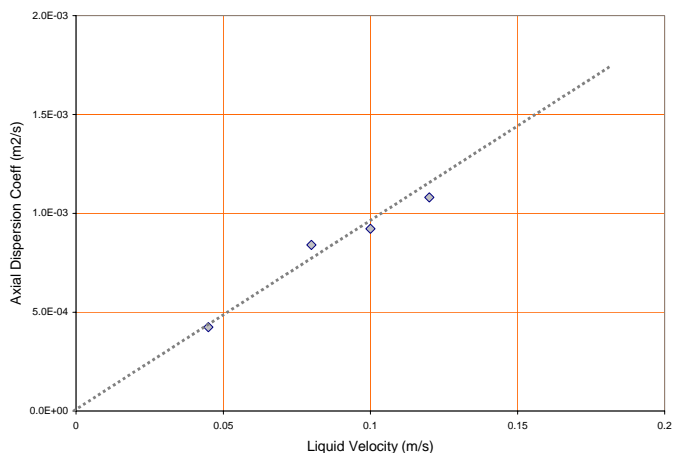
Figure 2. Liquid phase axial dispersion in HyperCat

Heat Transfer. The heat transfer coefficient of the HyperCat system was modeled using the gas-hold and liquid-phase dispersion data. The presence of gas bubbles in the heat-transfer zone allows continuous replacement of the liquid film in contact with the heat-exchanger surface leading to heat transfer rates which are similar to that obtained in a bubble column reactor under comparable gas velocities. However, since HyperCat system will operate at higher gas velocities than that possible in a slurry bubble column system, the heat transfer coefficient will be higher for the HyperCat system.

Catalyst Performance. A major stumbling block in converting structured carriers into structured catalysts is that for the same amount of active catalyst loading, structured catalysts give much lower activities than traditional powder catalysts[6].
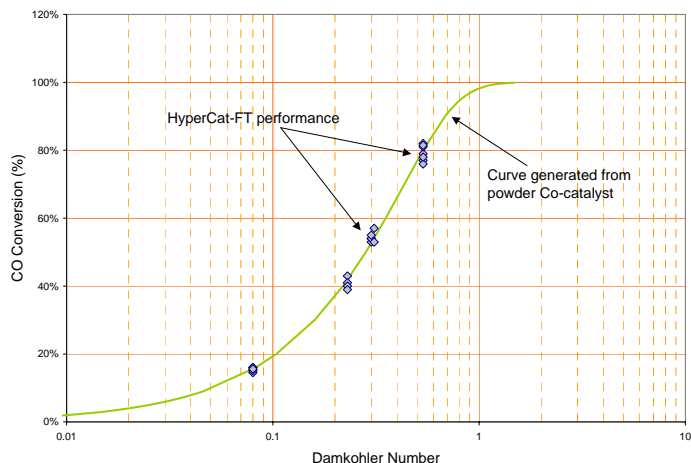

Figure 3. HyperCat-FT catalyst performance compared to powder FT catalyst

To ensure that we did not run into the same problem, we synthesized a powder catalyst (100μ diameter) and a HyperCat-FT catalyst using Cobalt as the active phase, Ruthenium as a promoter and γ-alumina as the support. We generated CO conversion versus Damkohler number (Da) curve using the following relationship[7]

$$Da = \tau\, k_{CO} = - (1/6) \ln (1 - x_{CO}) + (1/3) x_{CO}$$

where τ is the residence time, k_{CO} is the 1st order rate constant and x_{CO} is the CO conversion.

It is very clear from the data shown in **Figure 3** that there is virtually no difference in the performance of the HyperCat as compared to the powder catalyst. Thus, we have established that the HyperCat system can match the performance of powdered catalyst on equivalent Cobalt loading basis. This result is extremely important in light of other efforts being made to develop structured catalysts for Fischer-Tropsch reaction, which show that the activity of the structured catalyst is always lower than the powder catalyst[8].

Comparison with slurry bubble column reactor. Finally, we studied the effect of liquid dispersion on catalyst performance by comparing the performance of the powder catalyst in a bubble column reactor with the HyperCat-FT system. As shown in **Figure 4**, the CO conversion is much lower for a low Peclet number (bubble column reactor with a back-mixed liquid phase) as opposed to a higher Peclet number for the HyperCat system. The tests were conducted under the same process conditions and Damkohler number. The change in Peclet number did not change the liquid product distribution or the methane selectivity – which appear to be mainly a function of reaction temperature and pressure.
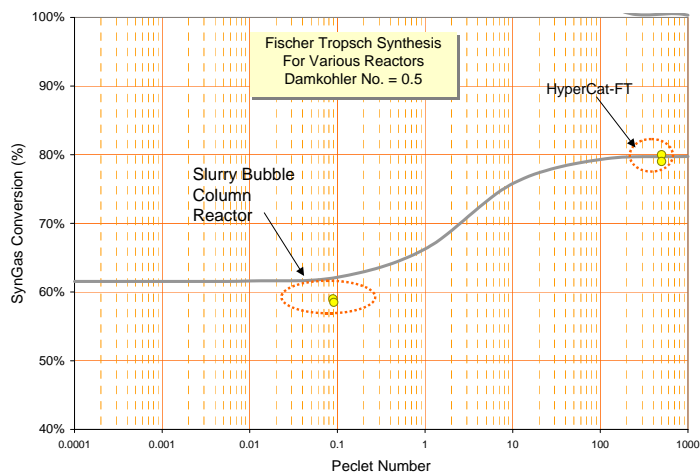

Figure 4. Effect of liquid phase axial dispersion on CO conversion

Conclusions

The Fischer-Tropsch reactor design challenge can be distilled down to the following critical issues:

(1) Achieve a high conversion per pass, in order to achieve high yields and reduce recycle and investment costs
(2) Eliminate the solids handling issue
(3) Provide high heat-transfer rates to remove the large reaction heat
(4) Minimize pore and film diffusion limitations

As seen from the above analysis issues 1 & 2 can be easily met in a fixed-bed reactor, while issues 3 and 4 are more suitable in a back-mixed bubble column reactor. However, one reactor alone is unable to satisfy all four requirements simultaneously. Exelus has developed a novel structured catalytic system that allows one to meet all four criteria in a single catalytic system. Hydrodynamic tests reveal that the HyperCat has similar gas-hold up as a slurry bubble column reactor but with a much lower liquid axial-dispersion coefficient. Modeling studies appear to indicate that the heat-transfer coefficient of this new system is similar to a bubble column reactor. Catalyst performance tests reveal that the performance of the HyperCat is similar to that of a powder catalyst when used in a plug-flow reactor.

References

(1) Dry, M.E. "The Fischer–Tropsch process: 1950–2000", Catalysis Today, 71 (2002)
(2) De Swart, J.W.A.; Krishna, R.; Sie, S.T., Selection, design and scale up of the Fischer-Tropsch reactor, Stud. Surf. Sci. Catal. 1997, 107, 213–218.
(3) Burtron H. Davis, "Overview of reactors for liquid phase Fischer–Tropsch synthesis", Catalysis Today, 71 (2002)
(4) Krishna, R., Van Baten, J.M., Urseanu, M.I. and Ellengerber, J., A scale up strategy for bubble column slurry reactors, Catalysis Today, 66, 199 - 207 (2001).
(5) Alexander, B. F. and Shah, Y. T. Axial dispersion coefficients in bubble columns. Chem. Engng J. (1976) 11, 153-156
(6) Liu, W. "Mini-structured Catalyst Bed for Gas-Liquid-Solid Multiphase Catalytic Reaction", AIChEJ, p1519-1532, July 2002
(7) Post, M.F.M., "Diffusion Limitation in Fischer-Tropsch Catalysts", AIChE J, 35, 1007-1114, 1989
(8) Hilmen, A., E. Bergene, O.A. Lindvåg, D. Schanke, S. Erib, A. Holmenc, "Fischer–Tropsch synthesis on monolithic catalysts of different materials", Catalysis Today 69 (2001) 227–232

CLEAN FUEL PRODUCTION USING PLASMA ENERGY PYROLYSIS SYSTEM (PEPS®)

Ron Patun, National Defense Center for Environmental Excellence (NDCEE), Johnstown, Pennsylvania
Jay Ramamurthi, EnerSol Technologies, Inc., Lorton, Virginia
Arthur Hartstein, U. S. Department of Energy (DOE), Washington, DC

Overview

Statement of Problem. The U.S. imports about sixty (60) percent of its fuel requirements (Energy Information Administration 2005) This figure is expected to increase to about 70 percent by the year 2025 (Energy Information Administration 2005). This reliance on foreign sources of oil has created both national and economic security issues for the U.S. This paper will discuss the use of the Enersol PEPS® gasification process for the production of syngas from petroleum coke (petcoke), which can subsequently be converted to clean transportation liquid fuels. This process, compared to syngas produced from natural gas, has the advantage of using petcoke, an oil refinery by-product, rather the expensive natural gas that will have to be imported. This is a technology transfer opportunity for the Department of Energy (DOE) and the Department of Defense (DoD) to increase the domestic source of environmentally friendly transportation fuels

Proposed Solution, Use of PEPS®. The U.S. produces over 30 million tons per year of petcoke, most of which has low economic value, at a number of refineries. The petcoke is a by-product of thermal cracking of crude oil. PEPS®, a novel Gasification Technology, which utilizes plasma energy technology, can be used to thermally convert petcoke to produce syngas. EnerSol Technologies, Inc. developed the thermal treatment process, which is accomplished in the absence of excess air. After gas purification occurs, the clean syngas can be used to produce clean fuels by further processing using conventional Gas-to-Liquid (GTL) technologies such as Fischer-Tropsch (F-T) technology. This technology is able to produce clean fuels with no sulfur for DoD and Industry applications. In addition, the PEPS® can be used to produce only hydrogen gas instead of syngas for fuel cell or transportation applications.

Introduction

History of Plasma Energy Technology. Plasma energy technology has been studied since the 1960's. The technology was originally developed for the aerospace industry to simulate the reentry conditions of space vehicles. The technology was also used by the specialty metals industry to produce high purity metals. During the 1980's, the Government funded considerable research to apply this technology for treating the most difficult-to-treat wastes produced by our society. There is high interest in plasma energy technology because of its ability to achieve temperatures near 10,000 degrees Celsius. Such high temperatures are sufficient to melt inorganic compounds and metals while thoroughly destroying all organic constituents.

Review PEPS® Technology and Prior Work. During the performance of an earlier Army funded task, the PEPS® was used to demonstrate positive Demonstration/Validation test results on the treatment of three surrogate waste streams. Tests were performed to measure both performance and environmental benefits. The National Defense Center for Environmental Excellence (NDCEE) provided monitoring and coordination support. EnerSol Technologies Inc. housed operated the demonstration unit that was designed and built from an earlier Army project. The results of the high-temperature gasification process were independently validated by the NDCEE, Weston Solutions, and outside laboratories. Building on the success of the original PEPS® task, the Army tasked the NDCEE/EnerSol team to design a PEPS® that could demonstrate energy recovery opportunities.

Process Description

Process Flow Diagram. The Process Flow Diagram for the Clean Fuels PEPS® is shown in Figure 1. The major process operations include: petcoke preparation and feeder systems, reactor vessel, plasma torch, slag removal, solids removal, energy recovery, syngas purification, and pressurization of the syngas to be delivered to the F-T processing unit.

Design Capacity and Estimated Syngas Production. The design of the prototype unit has been established for a petcoke feed rate of 25 tons per day. Steam will be added to the reactor vessel to provide a source of hydrogen because petcoke has very low hydrogen content. In addition, oxygen gas is added to provide a source of oxygen for conversion to the carbon monoxide and dioxide. This system is designed to produce about 1,700 scfm of clean syngas.

System Description

Feedstock Handling. The feedstock handling equipment will provide crushing, screening, safe movement and feeding of the petcoke at the site. Safety and performance issues require: movement of the petcoke from the storage site to the feedstock handling without producing dust or particulate emissions, reduction of the size of the petcoke to meet the conversion required in the reactor, weighing the petcoke to establish actual throughput, and a means to physically introduce the waste into the reactor.

Plasma Reactor. The plasma reactor is designed to maximize petcoke conversion while minimizing fine particulate carryover with sufficient volume and gas phase residence time for petcoke conversion to syngas. Sufficient volume and residence time will be provided for the vitrification of inorganic components of the petcoke, which is tapped from the molten slag bath at the bottom of chamber. The selected inside lining material (refractory) will be designed to withstand a maximum processing chamber temperature of about 1650° Celsius and the corrosive nature of the gases produced. The reactor will have several penetrations/openings for torch mounting, solid feed, preheat burner, view ports, slag tap, exhaust gas discharge, and instrumentation. The steel and refractory will be designed to meet mechanical strength requirements.

Plasma Heating System (PHS). The plasma torch contained in the Plasma Heating System (PHS) provides the energy to produce the high temperature required for destruction of organic materials and the melting of inorganic materials. Design features of the PHS include: interface with the refractory-lined reactor, capability of remote operation, compatibility with both highly organic and inorganic components of petcoke, and ability to deliver heat energy to the reaction chamber in a safe manner. The PHS includes components such as a power supply, an arc starter, a plasma arc torch, a torch positioning system, a plasma gas supply, and a torch cooling system. The PHS torch is compatible with the processing chamber operating conditions and gas environment and is of appropriate size and power rating to process both the organic and inorganic components. In addition the PHS was designed to minimize operating costs and emissions, has high turn down capabilities, operates at lower loads, operates reliably with long life

and minimal maintenance, and has high thermal efficiency (low heat losses).

Solids Removal. According to process model calculations, approximately 20 lbs/hr of particulate matter exits the reactor in the syngas stream. This amount of particulate matter is excessive for the efficient operation of energy recovery equipment and will be reduced significantly from the gas stream before entering a heat exchanger.

Energy Recovery. Energy recovery operations will be utilized to recover a percentage of the heat energy available in the raw syngas stream. The energy could be used to produce electricity for the torch or for oxygen production. Water or steam is required as a process additive to the reactor to achieve optimum conversion of the petcoke to syngas. The simplest form of energy recovery is accomplished by producing superheated steam. This reduces the energy required by the plasma torch. The heat recovery system is designed to withstand 1,100°C syngas temperature, produce superheated steam, cool the syngas to approximately 370°C, function reliably with minimal downtime, accommodate the particulate loading in the syngas, and resist corrosion from contaminants in the syngas.

Syngas Purification. The syngas purification system is designed to purify or clean the syngas produced in the PEPS® reactor to meet the purity requirements of the F-T process. In addition, any by-products, such as wastewater, must meet applicable emissions limits, which are determined by the site, and both local and state requirements. The overall performance of the syngas purification system is driven by gas flow, gas composition, temperature and pressure. The expected conditions at the inlet to the syngas purification system are 1,700 scfm of syngas at a temperature of 1,370 degrees Celsius with a pressure requirement of either atmospheric or 50 pounds per square inch (psi). The Syngas Purification system will perform a variety of functions during systems operation including the removal of carbon, inorganic oxides, and heavy metal particulates. Some of these particulates are detrimental to the downstream catalyst bed. In addition, no particulate is desirable in the F-T process. The purification system is designed to remove sulfur compounds and nitrogen, both of which are detrimental to the life of the catalyst bed. Acid gases such as HCl may be present in small quantities and must also be removed.

Control Logic. The control system is being designed and configured to ensure safe and reliable operation of the equipment and subsystems using robust industrial computers. The hardware architecture and software configuration employ modular structures for ease of troubleshooting and maintenance. The control strategies, interlocks, and sequences are being developed with input from equipment suppliers and independent reviewers. A Hazard and Operability (HAZOP) review will be performed on this system, to ensure robust, reliable and fail-safe operations.

Syngas Pressurization. To meet the pressure requirement of the F-T process, the syngas must be compressed after exiting the syngas purification system. If the syngas is partially pressurized prior to the syngas compression equipment, the size of the reactor and other equipment will be reduced and compression (capital and operating costs) will be less expensive. The syngas compression equipment will be required to provide clean syngas to the F-T process that could operate at pressures of from 300-500 psia depending on the catalysts used in the F-T process. Compression of gases containing hydrogen is difficult due to the effects that hydrogen has on most metals. These effects are metal dusting and hydrogen embrittlement, which are detrimental to most metals and have a tendency to reduce the life of equipment. Therefore, the syngas compression equipment must be compatible with hydrogen gas.

Advantages of Using PEPS® Technology for Petcoke Gasification. The main drivers behind this technology are:

- PEPS® technology can convert low value by-products from oil refineries into clean syngas
- The clean syngas can be used to produce clean fuels
- Production of alternate clean fuels is essential to maintaining national security
- PEPS® technology has been proven to be effective for treatment of hazardous wastes and Risk Reduction Testing is planned to evaluate the amount and quality of syngas produced from petcoke samples or surrogates.
- All emissions are controlled. Off-gases meet Clean Air standards, wastewater is treated for safe discharge, and residual slag passes Toxicity Characteristic Leaching Procedure (TCLP) standards.

Disclaimer. The views, opinions, and/or findings contained in this paper are those of the authors and should not be construed as an official Department of Army position, policy, or decision unless so designated by other official documentation.

Reference
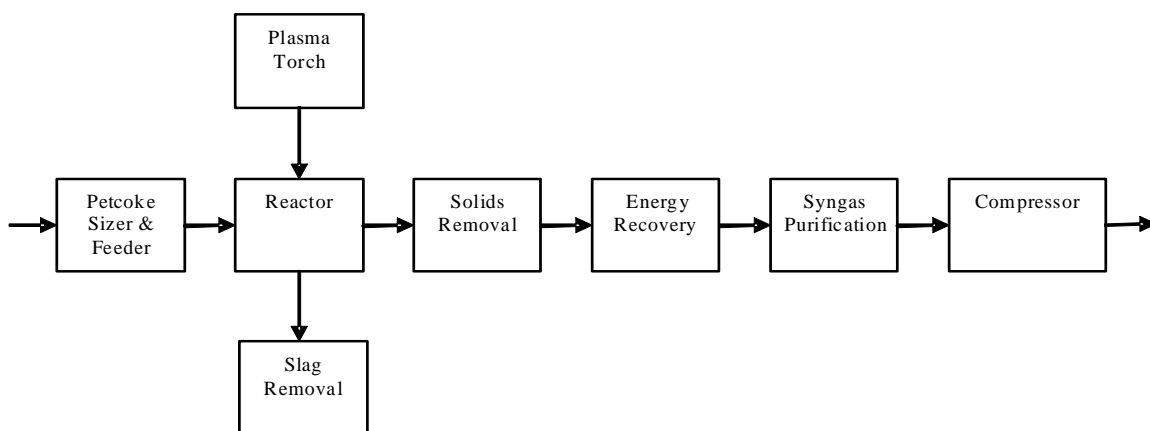Energy Information Administration, Annual Energy Outlook 2005, http://www.eia.doe.gov/oiaf/aeo/overview.html, 4/25/05

Figure 1. Process Flow Diagram

SCREENING OF POTENTIAL O-RING SWELLING ADDITIVES FOR ULTRA-CLEAN TRANSPORTATION FUELS

John P. Baltrus[1], Dirk D. Link[1], Paul H. Zandhuis[2], Robert J. Gormley[1]

[1] U.S. Department of Energy, National Energy Technology Laboratory, P.O. Box 10940, Pittsburgh, PA 15236-0940

[2] NETL Site Support Contractor, Parsons RDS, P.O. Box 618, South Park, PA 15129

Introduction

The primary components of Fischer-Tropsch (F-T) fuels are typically linear and branched alkanes.[1] As such, they will require additives in order to exhibit the properties of their petroleum-derived counterparts that are critical for use in transportation applications. Among the most important properties are lubricity and seal swelling capability.[2-4] A near-term solution to the seal swelling and lubricity deficiency of F-T fuels is blending the F-T fuel with conventional petroleum-derived feedstocks.[4] Unfortunately that solution negates many of the benefits derived by using a pure ultra-clean transportation fuel. For the same reason, addition of sulfur compounds, which would induce the desired lubricity properties, is not an option. Therefore other classes of compounds, specifically aromatics and oxygenates, are being investigated as additives to induce the desired properties. This study specifically deals with attempts to determine which classes of compounds are most efficient at promoting nitrile rubber o-ring swelling. Of particular interest is the determination of what specific compounds induce the greatest amount of swelling per unit weight or volume.

Experimental

Swelling studies. The swelling properties of the fuels were measured using ASTM Methods D-1414 and D-471. The o-rings used in the studies were buna-N (nitrile) N0602-70, obtained from Parker Seals, and having an o.d. and thickness of approximately 1.9 mm and 0.3 mm, respectively. Measurements were simultaneously conducted on three o-rings, as prescribed by the ASTM methods, in approximately 40 mL of fuel with an immersion time of 48 hours.

Extraction of Fuels. Extractions were performed using methanol in a procedure that has been previously described.[5] Briefly, the methanol-soluble components were extracted from the fuel and recovered in the methanol layer. This layer was isolated either for direct analysis or was further processing to isolate target analytes from co-extracted components using an HPLC separation method.[5]

Compositional Analysis. Analysis was performed with an Agilent GC-MS system (Agilent 6890 GC coupled to an Agilent 5973 Mass Selective Detector). Depending on the information desired, either a 100% non-polar column (Petrocol-DH 50.2, Supelco) or a polar column (Stabilwax-DA, Restek) was used. The polar column was used primarily for the analysis of extracts to help isolate polar components from the non-polar bulk matrix. Peak identification was performed using Agilent's ChemStation processing software against an NIST library of compounds, with additional confirmations obtained using the AMDIS software package.

Results and Discussion

Base measurements were conducted on petroleum-derived and F-T diesel and jet fuels. The results are reported in Table 1. As expected, the petroleum-derived fuels provided excellent seal swelling while the F-T fuels yielded poor swelling results.

Table 1. Swelling Results for Nitrile Rubber O-Rings in Various Fuels

Fuel	Volume Change (%)
Diesel – BP	16.2 ± 0.4
JP-5	14.0 ± 0.3
F-T Diesel	0.8 ± 0.1
F-T Jet (S-5)	0.6 ± 0.0
S-5 + 10% EI-037	8.5 ± 0.2
S-5 + 15% EI-037	13.6 ± 0.1
S-5 + 25% EI-037	25.4 ± 0.3
S-5 + 15% Aromatic 150	9.6 ± 0.5

A previous study attempted to determine the appropriate levels for spiking a synthetic jet fuel (S-5) with an aromatic-containing jet fuel (JP-5) or surrogate to induce acceptable levels of swelling of nitrile rubber o-rings.[6] It was determined that it required a greater volume of an aromatic solvent mixture, Aromatic-150 (ExxonMobile), to induce a given level of swelling than it did a petroleum-derived jet fuel to induce the same (or greater) degree of swelling. Specifically, a 30 % blend of Aromatic-150 in S-5 was required to induce the same degree of swelling that a 20 % blend of JP-5 in S-5 induced.[6] These results indicated that while aromatic species are able to induce swelling, some species (or combination of species) present in the petroleum-derived fuel were more proficient in swelling than the aromatic species in the Aromatic-150 solvent.

The S-5 jet fuel was blended with various concentrations of the Aromatic-150 solvent and a highly-aromatic coal-derived jet fuel precursor, EI-037 (Energy Research Institute, Pennsylvania State University), to determine what amount of blending agent would be required to achieve the swelling level imparted by a JP-5 fuel. The results are reported in Table 1. At least 15 volume percent of the blending agents was found to be required, with the coal-derived jet fuel having the greatest impact on swelling.

A comparison of Aromatic-150 and JP-5 was made using GC-MS with a 100% non-polar analytical column. The results showed that the region of overlap between Aromatic-150 and JP-5 ended at approximately the point where dodecane eluted. Therefore, it was inferred that whatever similar compounds in the two liquids may be responsible for swelling had to be present in the lower-boiling fraction of the petroleum-derived fuel.

The JP-5 fuel was then fractioned at specific cut-points to yield fractions with different classes of organic compounds in an effort to determine which classes of compounds induced the most swelling. For instance, the fraction of a JP-5 fuel with boiling point less than that of dodecane (212°C) induced considerably more swelling of nitrile rubber o-rings than the fraction with boiling point greater than 212°C (16.4 % vs. 9.2 %). The lower boiling fraction primarily contained single-ring aromatic compounds (alkylbenzenes), a small amount of naphthalene, and alkyl phenols, which are suspected swelling agents.

Another attempt to identify the species contained in JP-5 that may be responsible for swelling was made by conducting switch-loading tests. The nitrile o-rings were swelled in JP-5 fuel and then transferred to a synthetic S-5 fuel where the o-rings subsequently shrunk. It was assumed that the shrinking released a representative combination of the components of the JP-5 fuel that were previously absorbed by the o-rings. The components released into the S-5 fuel were then determined using methanol extraction followed by GC-MS analysis. The most prominent oxygenates were diethylene glycol

monomethyl ether (diEGME) and diethylene glycol monobutyl ether (diEGBE). Other species detected included naphthalene and two methylnaphthalene isomers. The GC-MS chromatogram for the extract is shown in Figure 1.
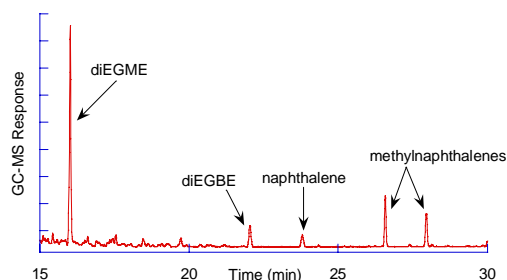

Figure 1. GC-MS analysis of a methanol extract of S-5 fuel after switch-load testing of o-rings immersed in JP-5 followed by immersion in S-5.

Both oxygenates were then tested separately for their ability to promote swelling of nitrile o-rings by spiking them at the 1% volume level in the S-5 fuel. The data in Table 2 indicated that both diEGME and diEGBE yielded poor swelling results. Others have tested the same compounds using optical ellipsometry to measure the degree of o-ring swelling and have reported a higher degree of sweling. The reason for the discrepancy is not understood, although the history of nitrile rubber may play a role in its susceptibility to swelling.

The coal-derived jet fuel precursor was characterized using an extraction method followed by GC-MS analysis to determine the most prominent aromatic compounds in the fuel. The results showed that naphthalene and naphthalene analogues were present in high concentrations. Naphthalene and some of its analogues were then tested as swelling agents at the 1% level in a synthetic S-5 jet fuel. The results are reported in Table 2. The compounds yielded very little swelling at that concentration, although additional tests of naphthalene at higher concentrations induced somewhat more swelling.

Based on the work of others[7], it was decided to further explore the use of Hansen Solubility Parameter (HSP) matching to predict which solvents would work best at inducing swelling in nitrile rubber. The solubility parameters are part of an approach for predicting polymer solubility based on the theory that the cohesive energy of a liquid is comprised of several individual forces. The main forces are D (dispersion), P (dipole interactions), and H (hydrogen bonding). Maximum solubility for the polymer is predicted when the D, P and H factor values are similar for the polymer and solvent. The HSP Handbook[8] was scanned for solvents whose parameters most closely matched those of nitrile rubber. Compounds containing sulfur and nitrogen functionalities were ignored because they would likely negate the environmental benefits of moving to ultra-clean fuels. Of the compounds that remained, the best HSP matches were found for oxygenates such as organic carbonates, lactones, plus select aldehydes, ketones and alcohols. Solubility issues were encountered with some of the compounds; specifically with those having a high hydrogen bonding factor. Results are reported in Table 2 for the compounds that were tested. It can be plainly seen that except for a couple of compounds, the enhancement in nitrile o-ring swelling was negligible.

Table 2. Swelling Results for Nitrile Rubber O-Rings in F-T Jet Fuel (S-5) Spiked With Various Organic Compounds

Fuel	Volume Change (%)
S-5 + 1% diEGME	1.7 ± 0.1
S-5 + 1% diEGBE	1.8 ± 0.1
S-5 + 1% (wt) Naphthalene	1.2 ± 0.2
S-5 + 6.4% (wt) Naphthalene	7.9 ± 0.3
S-5 + 1% Tetralin	0.9 ± 0.0
S-5 + 1% Decalin	0.8 ± 0.1
S-5 + 1% Propylene Carbonate	1.9 ± 0.2
S-5 + 1% Ethylene Carbonate	1.1 ± 0.2
S-5 + 1% Vinylene Carbonate	1.8 ± 0.2
S-5 + 1% γ-butyrolactone	2.4 ± 0.1
S-5 + 1% ε-caprolactone	4.6 ± 0.0
S-5 + 1% acetyl-acetone	2.6 ± 0.1
S-5 + 1% Allyl Alcohol	6.0 ± 0.1
S-5 + 1% Tiglic Aldehyde	2.3 ± 0.1
S-5 + 1% Methyl Vinyl Ketone	2.9 ± 0.1
S-5 + 1% Phenol	15.4 ± 0.4
S-5 + 1% 1,2,3,4-tetrahydro-1-naphthol	4.6 ± 0.0
S-5 + 1% 5,6,7,8-tetrahydro-1-naphthol	7.3 ± 0.2
S-5 + 1% 2-tert-butyl Phenol	8.9 ± 0.0
S-5 + 1% 2,4-dimethyl Phenol	12.8 ± 0.2
S-5 + 1% 2-ethyl Phenol	13.5 ± 0.2

The initial pretext for looking more closely at HSP matching to predict which compounds would be most active for o-ring swelling was the very good swelling that was observed for nitrile rubber when phenol was added to S-5.[8] It was observed that the HSP for phenol was fairly close to that for nitrile rubber and therefore it was suggested that the HSP might be a good predictor of nitrile solubility (swelling). Because phenol yielded such favorable swelling results, along with the fact that previous analyses of JP-5 fuel indicated that the most abundant oxygenates in the fuel were alkylphenols, it was decided to examine other phenol analogues. The results are reported in Table 2. All the phenol analogues yielded enhanced swelling. The relative degree of swelling was the least when two-ring structures were used and when a tert-butyl group was added to the phenol. A greater degree of substitution on the ring also yielded progressively poorer results compared with a non-substituted phenol, indicating that perhaps steric effects outweigh electronic effects in determining the ability of the phenol to induce swelling.

Conclusions

Through the use of switch-loading tests and an analytical method based on methanol extraction followed by GC-MS analysis, several possible compounds were identified for individual testing as possible swelling agents for synthetic fuels in contact with nitrile rubber. These compounds included naphthalenes and alkyl phenols. Another empirical method based on matching of Hansen Solubility Parameters also was used to identify additional candidate compounds to promote swelling of synthetic fuel. Of the compounds tested, phenol and its analogues provide the greatest degree of swelling per volume of the compound added to the fuel. Steric factors appear to limit the ability of the phenol analogues to promote swelling. Still to be examined is the possibility that synergistic effects may take place between certain classes of compounds.

JP-5 fuel. Reference to any specific commercial product, process or service is to facilitate understanding and does not imply its endorsement or favoring by the U.S. Department of Energy.

References
(1) Cookson, D. J; Smith, B. E. *Fuel* **1989**, *68*, 776.
(2) Anastopoulos, G.; Lois, E.; Zannikos, F.; Kalligeros, S.; Teas, C. *Fuel* **2002**, *81*, 1017-1024.
(3) Morgan, P.; Viljoen, C.; Roets, P.; Schaberg, P.; Myburgh, I.; Botha, J.; Dancuart, L. *SAE Technical Paper No. 982488* **1998**.
(4) Chang,, P. H.; Colbert, J. E.; Hardy, D. R.; Leonard, J. T. *Prepr. Pap.-Am. Chem. Soc., Div. Pet. Chem.* **2004**, *49* (4), 414-417.
(5) Link, D. D.; Baltrus, J. P.; Zandhuis, P. H.; Hreha, D. C. *Prepr. Pap.-Am. Chem. Soc., Div. Pet. Chem.* **2004**, *49* (4), 418-421.
(6) Harrison, W. III; Graham, J.; Minus, D.; Striebich, R. *results presented at the* Coordinating Research Council (CRC) Aviation Meeting, Alexandria, VA **2004**.
(7) Graham, J. L.; Striebich, R. C.; Minus, D. K.; Harrison, W. E. III *Prepr. Pap.-Am. Chem. Soc., Div. Pet. Chem.* **2004**, *49* (4), 435-439.
(8) Hansen, C. M. *Hansen Solubility Parameters, A User's Handbook*, CRC Press, Boca Raton, FL, 2000.

ITM CERAMIC MEMBRANE TECHNOLOGY TO PRODUCE SYNTHESIS GAS

Christopher F. Miller*[1], Michael F. Carolan[1], Christopher M. Chen[1], Eric Minford[1], William E. Waldron[1], James J. Steppan[2]

[1.] Air Products and Chemicals, Inc.
7201 Hamilton Blvd
Allentown, PA, 18195 USA

[2.] Ceramatec, Inc.
2425 South 900 West
Salt Lake City, UT, 84119 USA

Introduction

Air Products and Chemicals and its partners are developing Ion Transport Membrane (ITM) technology for the production of hydrogen and carbon monoxide (synthesis gas or "syngas"). The ITM Syngas process is a breakthrough technology that combines air separation and high-temperature synthesis gas generation processes into a single ceramic membrane reactor, with significant savings in the capital cost of synthesis gas production. Because synthesis gas is a feedstock for a range of different processes, ITM Syngas represents a technology platform that has numerous applications, such as hydrogen, clean fuels and chemicals.

Discussion and Results

ITM ceramic membranes are fabricated from non-porous, mixed-metal oxides and operate with exceptionally high oxygen flux and selectivity when exposed to an oxygen chemical potential gradient at high temperatures. A conceptualization of the ITM Syngas technology is shown in Figure 1. Oxygen from low-pressure air diffuses to the membrane surface where it adsorbs, dissociates and forms oxygen anions. The anions permeate through the dense ceramic membrane along the oxygen anion sublattice to the other side which contains high-pressure natural gas and steam. The oxygen anions are discharged into the reducing atmosphere and react with natural gas in a partial oxidation process to produce hydrogen and carbon monoxide. There is a balance flux of electrons through the membrane to complete the electrical circuit.

For the ITM Syngas process to be commercially viable, the membrane must have sufficient creep resistance, mechanical strength and thermodynamic stability in air, syngas and any contaminant environments. The family of materials which has been carefully designed to meet these requisite properties is perovskites with the formula $(La_{1-x}Ca_x)_yFeO_{3-\delta}$ where $0<x<0.5$, $y>1.0$ and δ makes the compound charge neutral. For example, Figure 2 shows the bending creep rate as a function of the A/B ratio, y, along with the grain size, for our ITM Syngas composition. The creep rate decreases by a factor of 2 as the A/B ratio increases from <1.0 to >1.0. This is notable since the test specimen for A/B>1.0 had smaller grain size, and the creep rate can increase significantly with decreasing grain size. Therefore, lower creep rates and longer membrane life can be obtained by using A/B>1.0 for the ITM Syngas materials.

Planar thin-film membranes with a microchannel design have also been fabricated from these materials that provide remarkable pressure handling capability and meet mechanical strength criteria, Figure 3. These membranes have achieved stable, high oxygen fluxes under process conditions due to their thin film structure and thermodynamic stability. Furthermore, as shown in Figure 4, commercial flux targets have been achieved with these membranes by meeting the aforementioned requisite properties, and also by advancing the reactor design to eliminate potential membrane contaminants.

This paper describes the development of the ITM Syngas ceramic membrane and the development of the reactor design, resulting in stable oxygen fluxes at our commercial target. Recent laboratory and pilot unit test results will be discussed, which will include oxygen flux data, an overview of reactor design modifications, and a comparison of membrane microstructure before and after flux testing.

Conclusion

Significant progress has been made in designing and manufacturing planar ceramic membranes, and in demonstrating targeted membrane oxygen fluxes, which are necessary steps toward commercializing the ITM Syngas technology. The potential economic benefits of the technology continue to be very promising.

Disclaimer

This paper was written with support of the U.S. Department of Energy (DOE) under Cooperative Agreement DE-FC26-97FT96052. The Government reserves for itself and others acting on its behalf a royalty-free, nonexclusive, irrevocable, worldwide license for Governmental purposes to publish, distribute, translate, duplicate, exhibit and perform this copyrighted paper.

Neither Air Products and Chemicals, Inc. nor any of its contractors or subcontractors nor the DOE, nor any person acting on behalf of either: 1. Makes any warranty or representation, express or implied, with respect to the accuracy, completeness, or usefulness of the information contained in this report, or that the use of any information, apparatus, method, or process disclosed in this report (Technology) may not infringe privately owned rights; or 2. Assumes any liabilities with respect to the use of, or for damages resulting from the use of such Technology.

Reference herein to any specific commercial products, process, or service by trade name, trademark, manufacturer, or otherwise, does not necessarily constitute or imply its endorsement, recommendation, or favoring by the DOE. The views and opinions of authors expressed herein do not necessarily state or reflect those of the DOE.
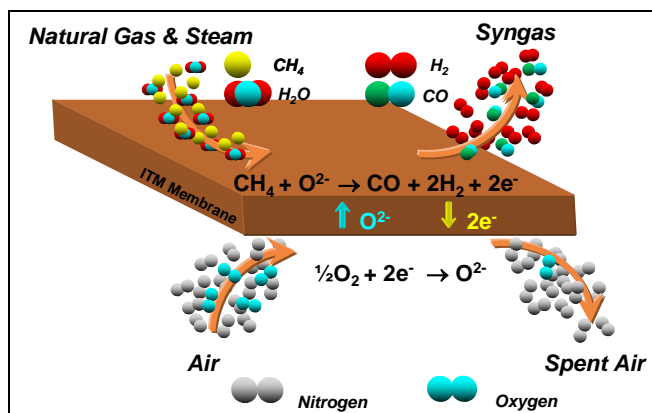

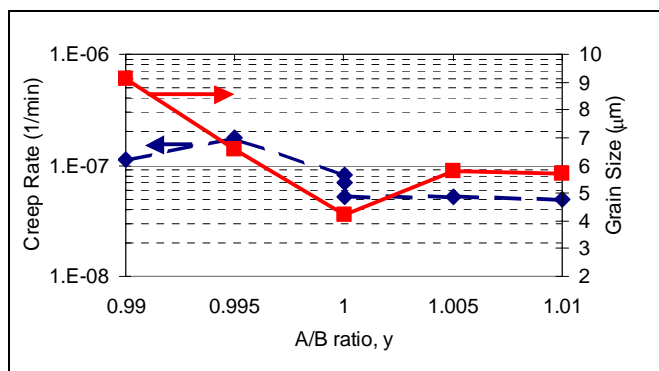**Figure 1.** Conceptual ITM Syngas Technology.

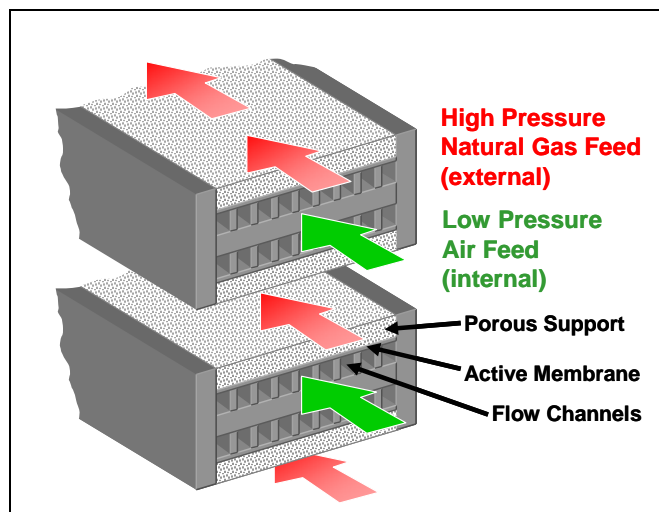**Figure 2.** Creep rate as a function of A/B ratio, y.

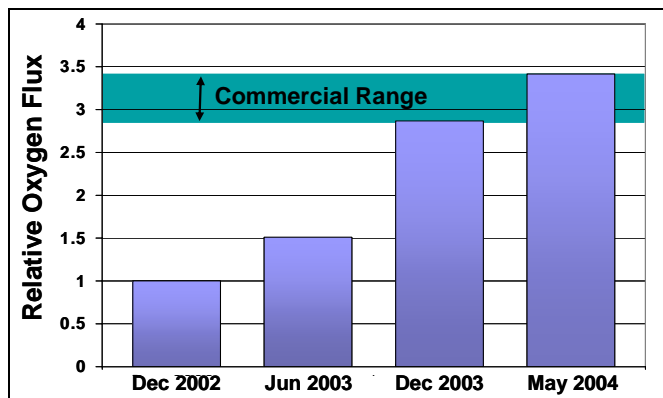**Figure 3.** Planar ITM Syngas membrane.

Figure 4. Advancement in oxygen flux performance.

THE EFFECT OF CO, H₂S AND H₂O ON THE HYDROGEN PERMEANCE OF PD-CU ALLOY MEMBRANES

Anthony Cugini, Bret Howard, Bryan Morreale, Osemwengie Iyoha, and Robert Enick

National Energy Technology Laboratory
U.S. Department of Energy
P.O. Box 10940
Pittsburgh, PA, 15236-0940

Introduction

Hydrogen is primarily produced through steam reforming of hydrocarbons or from coal gasification. Hydrogen production from coal gasification can provide a transition to the hydrogen economy as a result of the large volume of produced hydrogen in addition to the large volume of carbon monoxide, which can be further directed to a shift reactor to increase the hydrogen yield. Conventional methods of hydrogen production from hydrocarbons produce hydrogen with other gaseous components such as CO, CO_2, H_2O, H_2S and various other side reaction products from which hydrogen must be purified.

Robust, dense, metal membranes, such as Pd-Cu alloys, have the potential to separate and purify hydrogen from impure gas mixtures. An important application of membranes would be the implementation to in-situ and post-gasifier applications. Figure 1 illustrates one example of a membrane technology integrated into a gasifier application to enhance hydrogen production.
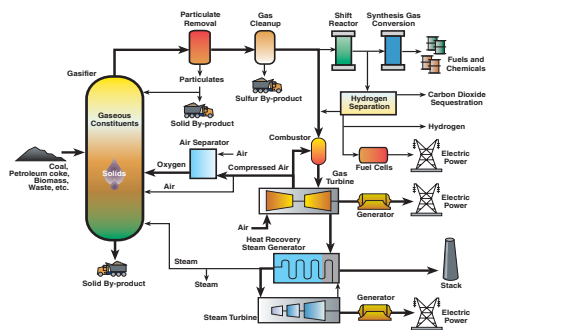

Figure 1. Integration of a hydrogen separation membrane into a gasifier application for the production of ultra-pure hydrogen from a coal-based gasification process.

Studies have shown that the integration of hydrogen membrane separation technologies into a gasification application improves the overall efficiency of the process as well as reduces the ultimate cost of the hydrogen product.[Parsons, 2003] However, the presence of various gaseous compounds may adversely affect the performance of metal membrane separations in these applications. For example, the presence of CO and H_2O in a H_2 feed stream was reported to reduce H_2 permeance through a Pd-Ag membrane by 40% and 70%, respectively [Hou, 2003]. Additionally, H_2S has been shown to diminish the permeance of Pd membranes [Edlund, 1993; ,McKinley, 1967; Edlund, 1994; Kajiwara, 1999]. Several research groups – including NETL – are exploring the viability of palladium alloy membranes (e.g. Pd-Cu) for gasifier and post-gasifier water-gas shift (WGS) membrane reactors and separators because of the relatively high hydrogen permeance of these alloys [Howard, 2004] and the H_2S-tolerance previously reported [Morreale, 2004; Edlund, 1993; McKinnley, 1967].

Results and Discussion

NETL has developed a Hydrogen Membrane Test (HMT) Unit for evaluating the performance of hydrogen separation membranes at elevated temperatures and pressures. This system is described in detail in previous publications [Howard, 2004; Morreale, 2004].

The viability of an 80wt%Pd-20wt%Cu alloy to purify hydrogen in the presence of impurities was assessed in the HMT by conducting diffusion experiments (of relatively thick membrane samples, generally between 100 and 1000 microns) in the presence of CO and H_2O at high-temperature and high-pressure conditions characteristic of a gasifier outlet stream, e.g. pressures up to 1.5 MPa and temperatures up to 1273 K [Iyoha, 2004]. The results for permeance of the membrane in the presence of equal volume mixtures of H_2-H_2O and H_2-CO are presented in Figure 2.
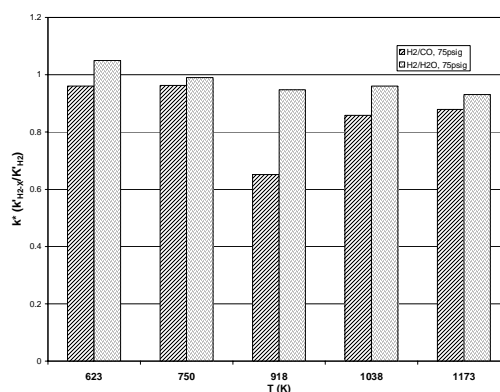

Figure 2. Impact of equal volume mixtures of H_2-CO and H_2-H_2O on the hydrogen permeance of the 80wt%Pd-20wt%Cu alloy at 75 psig. k*, a normalized performance value, is equal to permeance (mols/m²/s/pa$^{0.5}$) in the presence of the mixed gas stream (H_2-CO or H_2-H_2O) divided by permeance in the presence of a neat H_2 feed.

Even though the membrane appears to be negligibly impacted by the presence of H_2O, SEM images revealed a significantly roughened membrane surface after H_2O exposure. Similarly, the membrane appears to tolerate the presence of CO in the feed gas, evident by the results illustrated in Figure 2.

Overall, the results indicate that H_2O has a negligible influence on membrane permeance, while the presence of CO is observed to slightly influence membrane permeance. This is most pronounced at 918 K where the Boudouard reaction ($2CO = C + CO_2$) is favored. The appreciable reduction in permeance (at 918 K) may be attributed to the significant deposition of carbon on the membrane surface at this temperature. However, it should be noted that the membranes operated stably for more than 720 hours in the presence of each of these contaminants. Additional testing is planned to investigate the effect of test conditions on the membrane surface. Furthermore, surface morphological changes of membrane candidates in the presence of harsh gasifier contaminants are currently being assessed. Analytical techniques, such as SEM/EDS, XPS and XRD analyses, are being used to evaluate the influence of contaminants on surface composition of alloy membranes candidates.

Previous published work had shown that Pd-Cu alloys of the right composition and right crystalline phase have the potential to operate in the presence of 1000ppm H_2S with negligible decreases in flux [Kamakoti, 2005]. In that paper, we reported that fcc-phase Pd-Cu alloys are resistant to sulfur in the gas phase (see Figure 3).
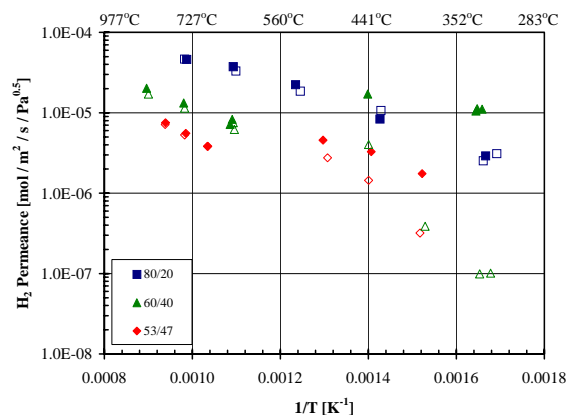
Figure 3. Permeance results of several palladium-copper alloys tested in the presence of 1000ppm H_2S as a function of temperature. Solid shapes represent results in the presence of neat hydrogen while open shapes represent the results in the presence of hydrogen-sulfide. Legend values are represented by: weight % palladium/weight % copper.

Currently, we are exposing coupons of Pd-Cu alloys (0, 53, 60, 80, and 100% Pd) to a flowing stream of H_2 with 1000 ppm H_2S to temperatures of 623 to 973K for different durations (1 h, 12 h, 25 h, and 7 days). These coupons are being analyzed by the aforementioned analytical techniques as well as gravimetric changes in an effort to characterize the effect of sulfur exposure on the alloy. The initial tests have already shown that each of the duration of sulfur exposure and the temperature can effect the surface composition, sulfur deposition, crystalline phase and morphology depending on the combination of time of exposure, temperature, and alloy composition. Additional tests are underway.

Conclusion

Pd alloy membranes have the potential of tolerating the impurities present in the production and separation of hydrogen from coal gasification processes. The impurities do appear to impact the surface for contaminant tolerant alloys but not in such a way as to significantly reduce the measured hydrogen flux.

Acknowledgement. This work was supported by the U.S. Department of Energy's Office of Fossil Energy

References
1. *Edlund, Friesen, Johnson, Pledger*, Gas Pur. and Sep. 8, 131 (1994).
2. *Edlund, Pledger*, J. Mem. Sci., 77 (1993) 255-264.
3. *Hou, et al*., Journal of Membrane Science 214, (2003) 43.
4. *Howard, et al.*, Journal of Membrane Science 241, (2004) 207.
5. *Iyoha et al*., AIChE Spring Meeting, Atlanta, GA, 04, 05.
6. *Kajiwara, Uemiya, Kojima*, Int. J. of Hydrogen Energy, 24 (1999) 839-844.
7. *McKinley, Nitro*, US Patent, 3,350,845 (1967).
8. *Morreale, et al*., Journal of Membrane Science 241, (2004) 219.
9. *Kamakoti et al*., Science, 307, 569 (2005).
10. *Parsons*. "Hydrogen Production Facilities - Plant Performance and Cost Comparisons," Final Report to DOE, Contract No. DE-AM26-99FT40465 (2002).

DIRECT DECOMPOSITION OF METHANE TO HYDROGEN ON METAL LOADED ZEOLITE CATALYST

Lucia M. Petkovic, Daniel M. Ginosar, Kyle C. Burch, and Harry W. Rollins

Idaho National Laboratory
P.O. Box 1625
Idaho Falls, ID 83415-2208

Introduction

The manufacture of hydrogen from natural gas is essential for the production of ultra clean transportation fuels. Not only is hydrogen necessary to upgrade low quality crude oils to high-quality, low sulfur ultra clean transportation fuels, hydrogen could eventually replace gasoline and diesel as the ultra clean transportation fuel of the future. Currently, refinery hydrogen is produced through the steam reforming of natural gas. Although efficient, the process is responsible for a significant portion of refinery CO_2 emissions. This project is examining the direct catalytic decomposition of methane over a metal modified zeolite catalyst as an alternative to steam reforming. The energy required to produce one mole of hydrogen is slightly lower and the process does not require water-gas-shift or pressure-swing adsorption units. The decomposition process does not produce CO_2 emissions and the product is not contaminated with CO – a poison for PEM fuel cells.

Experimental

The acid form of a commercially available zeolite was co-impregnated with two metal precursors by the incipient wetness technique. The material was dried at 393 K for 2 hs. Five hundred milligrams of the dried material were loaded in a tubular quartz reactor, calcined under flowing air (Zero grade, US Welding) for 4h at 873 K, then for 0.5 h at 973 K, and reduced under flowing hydrogen for 0.5 h at 573 K. The temperature was increased to reaction temperature and a flow of 20 cm^3/min of pure methane (99.99%, Scott Spelcialty Gases, PA) was initiated. Product yields as a function of time on stream (TOS) were measured on a Hewlett Packard 5890 gas chromatograph equipped with both FID and TCD detectors and Carboxen 1010 Plot and Petrocol columns.

To regenerate the catalyst, a flow of air was passed for 1 h through the catalyst bed kept at 873 K. A second set of experiments was performed over the regenerated catalyst.

Catalyst characterization. B.E.T. surface areas and micropore volume were determined on a Quantachrome Autosorb 1-C apparatus at liquid nitrogen temperatures. The carbonaceous material deposited on the catalyst was characterized by temperature-programmed oxidation (TPO) on a Perkin Elmer Diamond TG/DTA microbalance under 100 ml/min flowing air. About 10 mg of sample were placed in the balance pan and heated from room temperature to 1073 K at 10 K/min. Transmission electron microscopy analyses were performed on a Philips EM 420 at 120kV.

Results and Discussion

Hydrogen yields as a function of TOS at different reaction temperatures are shown on Figure 1. Other reaction products (not shown) included benzene and higher aromatics. At 873 and 973 K the production of hydrogen was relatively stable but at 1073 K a marked decrease was apparent.

The catalyst samples were regenerated in flowing air at 873 K. This temperature was chosen to avoid volatilization of metal oxide species during regeneration. After regeneration, catalyst activity was recovered. However some loss was apparent particularly on the

catalyst utilized at the highest reaction temperature. This loss of activity after regeneration may be ascribed to some carbonaceous deposits that may remain on the catalyst surface after regeneration.
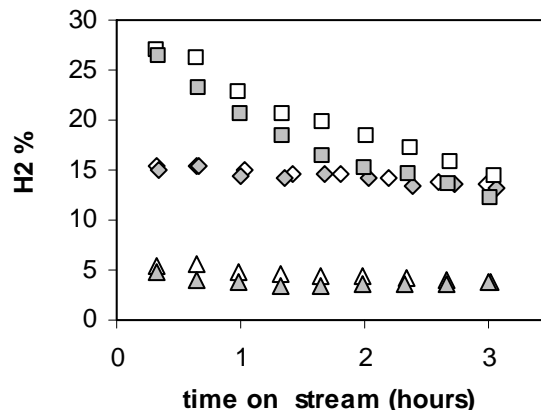

Figure 1. Hydrogen yields at 873 (triangles), 973 (diamonds), and 1073 K (squares) as a function of TOS. Hollow and filled symbols correspond to first and second set of reaction experiments, respectively.

Carbonaceous deposits were confirmed by the TPO studies as shown in Figure 2. The carbonaceous species deposited on the catalyst surface were more condensed as the reaction temperature increased, as expected. This is inferred from the higher temperatures necessary to oxidize and decompose the carbonaceous deposits during the TPO experiments. The carbonaceous deposits on the catalyst sample utilized at 873 K had desorbed completely at 873 K. However, temperatures as high as 973 K were necessary to desorb the carbonaceous material from the sample utilized at 1073 K.
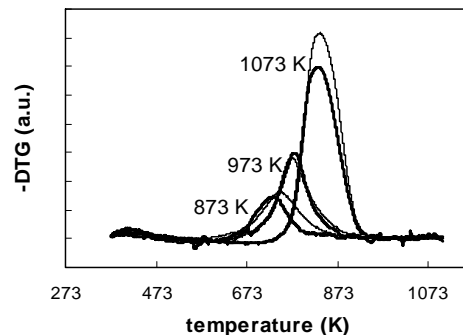

Figure 2. TPO profiles. Reaction temperatures are indicated. Thin and thick lines correspond to first and second set of reaction experiments, respectively.

For the TOS utilized in this study, the catalyst retained a high portion of its initial surface area and micropore volume as shown in Table 1. Transmission electron microscopy analyses showed a homogenous covering of the zeolite surface with carbonaceous deposits.

Table 1. Nitrogen Physisorption and TPO Results

Sample	BET SA (m^2/g)	MPV (cm^3/g)	% C
Fresh	403	0.12	–
873 K	407	0.13	3.1
973 K	310	0.10	4.5
1073 K	216	0.07	11.1

Li et al.[1] have reported that zeolite-supported nickel catalysts when utilized until complete deactivation produced 119 and 480 mol H_2/mol Ni, for ZSM5 and MCM22, respectively. The catalyst studied here deactivated slowly during long-term experiments and even at 30 h TOS the percentage of hydrogen was still above 6%. In this case, the integrated production was about 1200 mol H_2/mol metal, which indicates a more favorable hydrogen production.

Conclusions

A favorable production of hydrogen from direct decomposition of methane was found on the catalyst studied here, when compared with nickel-zeolite supported catalysts. Reaction temperature had a strong influence on catalyst regeneration. The catalyst utilized at 873 and 973 K could be regenerated without any significant loss of activity by calcination in air at 873 K. When the catalyst was utilized at 1073 K, a faster decrease in activity was found and the recovery of activity by regeneration was lower.

References
(1)   Li, J.; Lu, G.; Li, K.; Wang, W. *J. Molec. Catal. A* **2004**, *221*, 105.

EFFECT OF ULTRASONIC IRRADIATION ON ENZYMATIC TRANSESTERIFICATION OF WASTE OIL TO BIODIESEL

Hong Wu, Min-hua Zong

Biotechnology Department, South China University of Technology, Guangzhou 510640, P. R. China

Introduction

Biodiesel(long-chain monoalkyl fatty acid esters), a renewable and green fuel, is made from vegetable or animal fats. At present, the high cost of biodiesel, of which the raw material amounts to 75%, prohibits its wide application. Compared with chemical method, enzymatic process[1,2] seems to be a promising alternative because of its mild reaction conditions, easy recovery of product, being free of chemical wastes and low demanding on raw materials, which makes it possible to use waste oil as substrate for enzymatic production of biodiesel.

Wastes edible oils, from restaurants and household disposals and being creating serious problems of environmental control and food safety, have been considered as good raw material for biodiesel production. Immobilized *Candida antarctica* lipase was found to be effective for the methanolysis of waste oil.[2,3] A three-step methanolysis protocol could be used to protect lipase from inactivation by methanol. Compared with one-step reaction, it needs a longer time to reach the reaction equilibrium. So, efforts should be made to increase enzymatic reaction rate. Reports on the enhancement of the activity of certain enzymes by applying ultrasonic irradiation on the enzymes[4,5] led us investigate its effects on the enzymatic transesterification of waste oil to biodiesel in a solvent free system.

Experimental

Materials. Waste oil was collected from the restaurant in South China University of Technology. The saponification value was 200.3 mg KOH/g, from which, the average molecular weight of the waste oil was known to be 840.2. Novozym 435 (lipase B from *Candida antarctica*, 164 U/g, 1unit corresponds to the amount of enzyme that produces 1 μmol methyl oleate from triolein per minute at 35 °C) was kindly donated by Novo Nordisk Co. (Denmark). Methyl palmitate, methyl stearate, methyl oleate, methyl linoleate, methyl linolenate and methyl heptadecanoate (as internal standard) were purchased from Sigma (USA). All other chemicals were also obtained commercially and of analytical grade. Ultrasonic irradiation experiments were carried out using a ultrasonic bath (Type NP-B-400-15; Newpower Co. Ltd., China).

Determination of power density. Power density at sample sites in the ultrasound bath was determined according to the method described by Barton.[6]

Reaction. The reaction was carried out in 50-ml flask capped with a septum, incubated at 40 °C and in the presence or absence of ultrasonic irradiation. The reaction mixture contained 66 U Novozym 435, 10 g waste oil and 0.38 g methanol (1 molar equivalent). Samples of 100 μl were periodically withdrawn and centrifuged (12000 rpm, 10 min) and the upper layer was mixed with methyl heptadecanoate for GC analysis. In the ultrasonic pretreatment experiment, Novozym 435 was immerged into 10 g waste oil and exposed to ultrasonic irradiation for a certain time.

Analysis. The methyl ester (ME) content in the reaction mixture was assayed with a GC2010 gas chromatography (Shimadzu Corp., Kyoto) using a flame ionization detector and a HP-5 capillary column (0.53 mm × 15 m, HP, USA). The column temperature was hold at 180 °C for 1 min, raised to 186 °C at 0.8 °C /min and kept for 1 min, then upgraded to 280 °C at the rate of 20 °C /min. Nitrogen was used as the carrier gas at 2 ml/min. Split ratio was 1:100 (v/v). The injector and the detector temperatures were set at 250 °C and 280 °C, respectively.

Results and Discussion

The use of an ultrasonic bath has the advantages of simplicity, low cost, and modest power outputs reducing the likelihood of localized heating effects with ultrasound probe and cuphorn systems. The most obvious limitations are that the operating frequency is normally fixed and power densities vary within the bath. Consequently standardization of sample locations is essential for comparative purposes. In our study, the water addition to the bath was as high as 230 mm from the bottom and the sample was fixed at the position of 180 mm from the bottom. The maximum power density with water as medium was obtained in the center and this location was used for all the following reactions. The power densities were 0.21W/ml, 0.28 W/ml, 0.36 W/ml and 0.48 W/ml, respectively, when the power outputs were 40 W, 60 W, 80 W and 100 W, respectively.

As can be seen in **Figure 1**, the reaction accelerated markedly with the increase in power output when it was below 80 W. Further increase in power output up to 100 W, however, resulted in little rise in conversion after reaction for 2 h and the ME content of the product was lower than 30% in spite of the higher initial reaction rate, suggesting partial inactivation of the enzyme. This has been proved by experiments showing that the enzyme retained only 81% of its original activity after being treated with ultrasonic irradiation at 100 W. However, the best result achieved was only comparative to the control which was carried out with shaking at 150 rpm. This is mainly due to the high viscosity of waste oil and little enhancement in mass transfer at low ultrasonic intensities and inactivation of enzyme at high ultrasonic intensities.
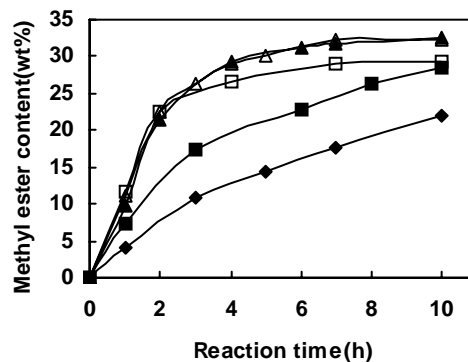

Figure 1. Effect of ultrasonic power on enzymatic transesterification of waste oil. The reactions were carried out at 40±2 °C in the presence of ultrasonic irradiation and the reaction mixture contained 10 g waste oil, 0.38 g methanol and 66 U Novozym 435. Control was carried out at 40 °C and 150 rpm. ◆,40 W; ■,60 W; ▲,80 W; □,100 W; △, control.

It has been reported that the reaction rate could be enhanced by pretreatment of enzyme with ultrasonic irradiation.[7] In our study, It was found that the reaction proceeded quite slowly during the first 1 hour of reaction as indicated by the low ME content of the reaction mixture (10.9%) and then accelerated. It seems that there exists a period for the enzyme to be activated. So, we speculated that

pretreatment of enzyme with ultrasonic irradiation might activate the enzyme and accelerate the enzymatic reaction. The results depicted in **Table 1** well supports the hypothesis.

Table 1. Effect of ultrasonic pretreatment on enzymatic transesterification of waste oil

Pretreatment means	Methyl ester content (wt%)
Ultrasonic irradiation	19.4
Shaking	12.1
Control*	10.9

Novozym 435 (66 U) was immerged into 10 g waste oil and then pretreated with ultrasonic irradiation (20 kHz, 80 W) at 40 °C for 30 min or with shaking at 40 °C and 150 rpm for 30 min. Methanol (0.38 g) was added to the reaction mixture and the reactions were carried out at 40 °C and 150 rpm for 1 h.
*Without pretreatment

Since the time enzyme was pretreated with ultrasonic irradiation could influence the reaction rate, effect of pretreatment time on the reaction was therefore investigated. As shown in **Table 2**, the reaction rate increased with increasing pretreatment time up to 30 min. Further increase in the pretreatment time, however, resulted in little change in reaction rate. So, the optimum pretreatment time was thought to be 30 min.

Table 2. Effect of ultrasonic pretreatment time on enzymatic transesterification of waste oil

Time（min）	Methyl ester content (wt%)
10	13.6
20	17.1
30	19.4
40	19.5
60	19.1

Novozym 435 (66U) was immerged into 10g waste oil and pretreated with ultrasonic irradiation (20 kHz, 80W) at 40°C for a certain period of time. Methanol (0.38g) was added to the reaction mixture and the reactions were carried out at 40°C and 150 rpm for 1 h.
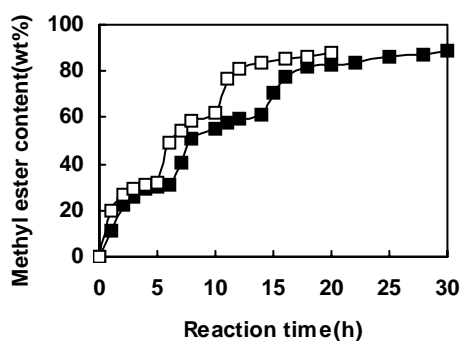

Figure 2. Time course of pretreated Novozym 435-catalyzed transesterification of waste oil. Reaction was performed at 40 °C, 150 rpm by adding 0.38 g methanol into the mixture containing 10 g waste oil and 66 U Novozym 435 pretreated or non- pretreated by ultrasonic irradiation (20 kHz, 80 W) at 40 °C for 30 min 0.38 g Methanol was added after 5 and 10 h or after 6 and 8 h and glycerol was rinsed with acetone after each step. □ , pretreated; ■ , non-pretreated.
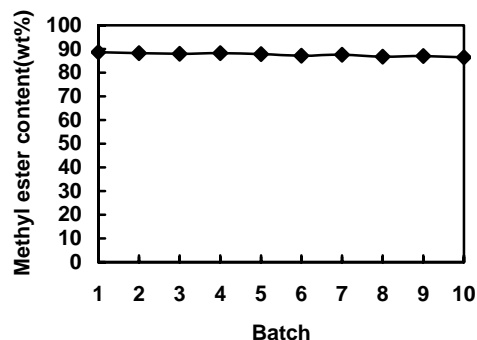

Figure 3. Operational stability of pretreated Novozym 435. Reaction conditions were the same as in Figure 2 and three steps served as one batch with a total reaction time of 20 h.

Figure 2 depicts the time course of pretreated Novozym 435-catalyzed transesterification of waste oil. During the three-step batch reaction, the reaction time of each step reduced to 5 h, 5 h and 10 h from original 6 h, 8 h and 16 h and one third of the total reaction time was saved. On the other hand, Novozym 435 pretreated by ultrasound showed good operational stability as indicated by a slight loss in activity after 10-batch operation (**Figure 3**).

Conclusion

Novozym 435-catalyzed transesterification of waste oil was markedly accelerated by pretreatment of the enzyme with ultrasonic irradiation at 20 kHz, 80 W for 30 min and Novozym 435 pretreated with ultrasonic irradiation showed good operational stability and so are potential for biodiesel production.

References
(1) Steinke, G.; Kirchhoff, R.; Muknerjee, K. D. *J. Am. Oil Chem. Soc.*, **2000**, *77* (4), 361-366
(2) Shimada, Y.; Watanabe, Y.; Sugihara, A.; Tominaga, Y. J. *Mol. Catal. B: Enzym.*, 2002, *17* (3-5), 133-142
(3) Wu, H.; Zong, M. H.; Lou, W. Y. *Chin. J. Catal*., **2004**, *25* (11), 903-908
(4) Vulfson, E. N.; Sarney, D. B.; Law, B. A. *Enzyme Microb. Technol*., **1991**, *13* (2), 123-126
(5) Sakakibara, M.; Wang, R.; Takahashi, R.; Takahashi, K.; Mori, S. *Enzyme Microb. Technol*., **1996**, *18*, 444-448
(6) Barton, S.; Bullock, C.; Weir, D. *Enzyme Microb. Technol*., **1996**, *18*, 190-194
(7) Zong, M. H.; Du, W.; Li, H. Q.; Liu, Y. *J South China Univ. Tech.*, **2000**, *28* (3), 101-104

EXSACT: NOVEL SOLID-ACID CATALYZED ISO-PARAFFIN ALKYLATION PROCESS

Mitrajit Mukherjee, Sankaran Sundaresan & Richard Porcelli

Exelus Inc., 99 Dorsa Avenue, Livingston, NJ 07039

Introduction

The recent ban on MTBE in several states (California, New York and Connecticut) has made it difficult for refiners to prepare gasoline blends that meet state and federal guidelines. EIA (Energy Information Administration) reports that the volume of total gasoline production can easily be restored to MTBE-free volume levels with alkylate. Alkylate is an ideal clean fuel component because it has a high octane rating, low vapor pressure and low toxicity. It is currently produced via iso-paraffin alkylation using as catalyst hydrofluoric acid (HF), which can be deadly if spilled, or sulfuric acid (H_2SO_4), which is also potentially harmful and increasingly costly to recycle. Exelus has developed an innovative iso-paraffin alkylation technology ExSact, as an economically viable alternative to HF/H_2SO_4 processes. The two main components of ExSact are:

1. A unique solid-acid catalyst that converts light hydrocarbons into alkylates &
2. A novel fixed-bed reactor that is designed to enhance the performance of this catalyst.

The synergistic integration of the "green" solid acid catalyst with the novel reactor is expected to provide refiners with a cleaner-by-design alternative to produce a high-octane gasoline component to meet both state and Federal requirements. This paper describes the successful development of this new "green" technology to produce alkylate.

Alkylation Background

Alkylation of isobutane with light (C_3–C_5) olefins in the presence of a strong acid catalyst involves a series of consecutive and parallel reactions occurring through carbocation intermediates[1]. The addition of proton to an olefin, followed by hydride abstraction from iso-butane, leads to a t-butyl cation. The t-butyl cation then combines with an olefin (say, C_4) to give the corresponding C_8 carbocation as shown in **Figure 1**. These C_8 carbocations may isomerize via hydride transfer and methyl shifts to form more stable cations. These C_8 cations undergo rapid hydride transfer as iso-butane regenerates the t-butyl cation to perpetuate the chain sequence.
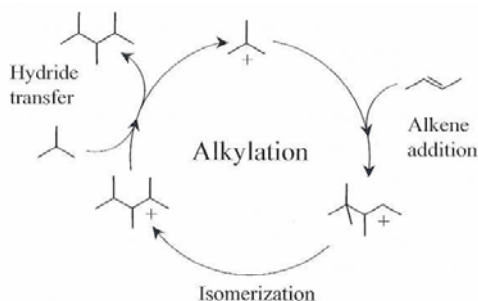

Figure 1. Simplified alkylation cycle[1]

Unfortunately, these are not the only reactions occurring during alkylation. There are a number of secondary reactions that, in general, tend to reduce the quality of alkylate. The C_8+ can continue to react with olefins and form larger cations. The successive addition of olefins to carbocations, or olefin polymerization, is the primary route to formation of large hydrocarbon residue or "coke", leading to catalyst deactivation.

Solid acid catalysts have been investigated as alternatives to liquid catalysts for isobutane alkylation for over 30 years[2]. These include $AlCl_3$; promoted zirconia; heteropolyacids, such as tungstates; liquid acids immobilized on silica, polymers, or other solid supports; and natural and synthetic zeolites. Solid catalysts can improve selectivity and reduce production costs, but their tendency to deactivate rapidly during alkylation has prevented virtually every known solid-acid alkylation catalyst from becoming commercially viable.

Exelus's Solid-Acid Catalyst Development

Using grants from the US Department of Energy and the National Science Foundation, Exelus started (in 2001) work on developing a viable solid-acid catalyst alternative to liquid acid catalyzed iso-paraffin alkylation technologies. Our goal was to develop a simple swing fixed-bed reactor process using a benign solid-acid catalyst. Our desire to use a fixed-bed reactor was influenced by two issues: a) to simplify process scale-up and b) to keep both capital costs and operating expenses as low as possible. This, however, is easier said than done for alkylation reactions. Iso-paraffin alkylation reactions are very fast and they suffer from severe pore diffusion limitations. As a result when catalyst particle sizes are increased from 100 μm (for slurry reactors) to 1.6 mm for fixed-bed reactors, the catalyst activity reduces by 10-fold as shown in **Figure 2**. To match the catalyst productivity of a slurry reactor, one would need to build a fixed-bed reactor with 10-times the volume – which is not practical for commercial scale system. In addition to using a fixed-bed reactor, we wanted to ensure that the solid-acid catalyst was both robust as well as benign i.e. environmentally friendly. We rejected right at the outset replacement of a liquid acid with a liquid-acid supported on solid particles or co-feeding toxic halogens or halogenated compounds to a solid-acid catalyst to maintain its activity.
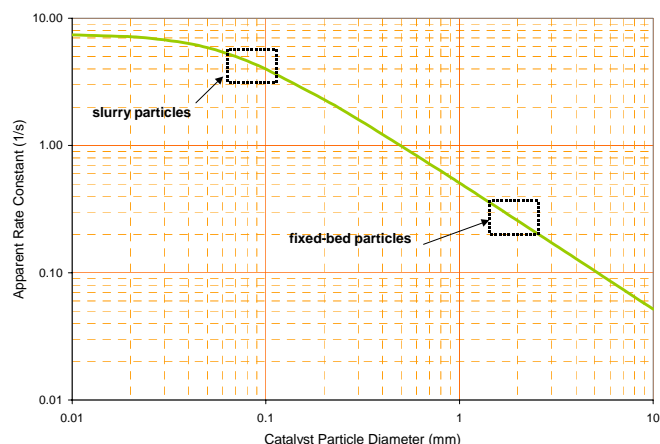

Figure 2. Reduction in catalyst activity with increasing particle size

Our development approach was to first understand the dynamics of the alkylation reaction by systematically studying the effect of both physical and chemical aspects of the solid-acid catalyst system design on product distribution and catalyst deactivation characteristics. Several different catalyst formulations encompassing a wide range of acid functions, number of acid sites and acid strengths were evaluated as part of this study. Many of our findings were in stark contrast to conventional (widely held) beliefs about solid-acid catalyzed alkylation reactions.

Through this systematic study, Exelus was able to identify an optimal "window" of design parameter values that were then used to develop the ExSact system. By judicious manipulation of the active material composition (number of sites and acid site strength), researchers at Exelus have developed a unique solid-acid catalytic system that has roughly 400% more active sites than a typical solid-acid catalyst. The catalyst activity of the solid acid was found to be higher than a typical liquid acid catalyst, which means that much lower amounts of catalyst are required to catalyze the iso-paraffin alkylation reaction, allowing one to design alkylation reactors with significantly lower volumes (hence cost).
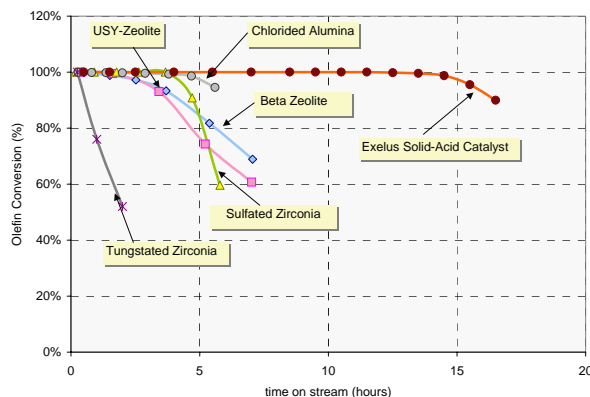

Figure 3. Exelus solid-acid catalyst performance compared to other commercially available systems

By integrating optimized acid-sites with superior mass transport characteristics and a pore architecture that reduces pore-mouth plugging, Exelus has developed a truly revolutionary solid acid catalyst. As shown in **Figure 3**, which compares the performance of Exelus solid-acid catalyst with other commercially available systems, the new catalyst system is easily able to achieve a quantum jump in performance over other solid-acid catalysts.

Novel Fixed-Bed Reactor Design

Through an extensive study of the solid-acid alkylation reactions, Exelus has developed a robust kinetic model that is able to predict product octane as well as catalyst lifetimes for a large range of reaction conditions. Kinetic analysis[3] revealed that the rate constant for the secondary (oligomerization) reaction is 2 orders of magnitude higher than the rate constant for the primary alkylation reaction. To achieve a substantial reduction in the rate of oligomerization, the olefin concentration (O) must therefore be kept 2 orders of magnitude lower than the iso-paraffin concentration (P). Kinetic analysis also revealed that the rate constant for the product degradation reaction is similar in magnitude to the rate constant for the primary alkylation reaction. By applying the kinetic model to novel reactor flow patterns, Exelus has been able to develop a unique fixed-bed alkylation reactor that enhances the primary reaction rate by optimizing both macro-mixing (residence time distribution) and micro-mixing (aggregate mixing) characteristics. The macro-mixing profile is optimized to reduce product degradation by minimizing the over-alkylation of iso-octane molecules to heavier (low octane) hydrocarbons. The desired micro-mixing characteristics (to achieve low olefin concentrations at the catalyst surface) are achieved by using proprietary turbulence enhancing devices called "Dispersion Accelerators."

The performance of the fixed-bed reactor was verified in Exelus laboratory over a period of 2 months through tests under commercially relevant process conditions. Product was sampled over

the entire length of the reactor to quantify the rate of alkylate degradation. **Figure 4** shows the results of this test.
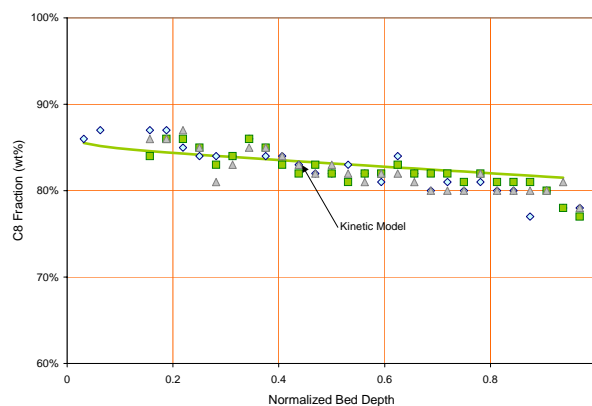

Figure 4. Performance of the Novel Fixed-Bed Alkylation Reactor

The kinetic model adequately describes the product composition for most of the reactor length. In effect, the yield of C8 alkylate is 20 wt% higher than that possible in a conventional recycle reactor, resulting in a net 1.5 octane number (RON) increase.

Comparison with Conventional Liquid Acid Processes

A comparison of the Exelus technology with competing liquid acid processes is presented below. We have used published data and pro-rated them (the sulfuric acid unit was pro-rated from a 7,500 bspd plant cost of $43.5 million while the HF plant was pro-rated from a 8,800 bpsd plant cost of $42.5 million) to reflect a plant capacity of 10,000 bspd.

Table 1. Comparison of the ExSact process with liquid-acid alkylation technologies

Parameter	ExSact Process	Hydrofluoric Acid Alkylation[4]	Sulfuric Acid Alkylation[5]
Plant Capacity (bspd)	10,000	10,000	10,000
Capital Expenses (million)	**$ 26**	**$ 46**	**$ 55**
Raw Material Consumption:			
Iso-butane Consumption	1.21 v/v olefin	1.2 v/v olefin	1.17 v/v olefin
Alkylate Yield	1.83 v/v olefin	1.8 v/v olefin	1.78 v/v olefin
Utility/Chemicals Consumption:			
Steam ($ 4/klb)	116,000 lb/hr	65,700 lb/hr	130,700 lb/hr
Power ($ 0.06/kWH)	600 kW	903 kW	4040 kW
Fuel ($ 4/MM Btu)	1.5 MM Btu/hr	47.7 MM Btu/hr	
Cooling Water ($ 0.05/gal)	12,740 gpm	15,750 gpm	15,600 gpm
Hydrogen ($ 0.55/lb)	70 lb/hr		
HF ($ 0.65/lb) or H_2SO_4 ($ 0.05/lb)	N/A	47 lb/hr	7920 lb/hr
Utility Costs ($/bbl)	**$ 1.40**	**$ 1.41**	**$ 2.90**

Investment costs are lower than liquid-acid technologies due to the following reasons:

1. Simpler reactor design using inexpensive materials of construction
2. Elimination of refrigeration equipment
3. No need for acid handling vessels

As a result, capital expenses to about $26 million for a 10,000 bbl/d plant – a reduction of 45-50% compared with hydrofluoric and sulfuric-acid alkylation processes.

Utility costs are about the same as an HF unit but significantly lower (about 50%) than a sulfuric acid plant for the following reasons:

1. Much lower power consumption
2. Inexpensive regeneration scheme using hydrogen

Finally, alkylate yields are higher due to elimination of acid-soluble oils that are formed during in liquid-acid catalyzed alkylation processes, resulting in lower feedstock consumption.

Conclusions

Exelus has developed a revolutionary refinery process (ExSact) that is designed to produce high-octane alkylate without the use of toxic liquid acids. The strength and distribution of its acid sites reduce olefin dimerization and paraffin cracking, while enhancing isobutane alkylation. Furthermore, the controlled pore structure of the catalyst reduces deactivation by coke formation and pore mouth plugging. The paraffin alkylation process using ExSact catalyst is fundamentally safer and cleaner than conventional liquid-acid catalyzed processes, eliminating the use and generation of toxic chemicals. Exelus has also developed a novel fixed-bed alkylation reactor to enhance the performance of the solid-acid catalyst. This new reactor uses innovative fluid dynamics and an unusual reactor residence time distribution designed to maximize alkylate production without sacrificing the product octane value. The innovations in the Exelus process are shown schematically in **Figure 5.**

The new solid-acid catalyst process promises significantly improved yields and selectivities, minimizing waste by-products and disposal problems associated with spent catalysts and regeneration of large quantities of liquid acids. Given the current push for eco-friendly processes to produce ultra-clean fuels, The ExSact technology is poised to fill a large void in the gasoline market for decades to come.

References

(1) Feller, A., Iker Zuazo, Alexander Guzman, Jan O. Barth and Johannes A. Lercher, *J. Catal. (216), 2003, 313-323*
(2) Corma, A.; Martinez, A. *Catal. Rev. Sci. Eng. 1993, 35, 483*
(3) Simpson M. F, Wei J, Sundaresan S, *Ind. Eng. Chem. Res. 1996; 35,3861-3873*
(4) UOP HF Alkylation Brochure, 2001
(5) Ackerman, Steve, Girish K. Chitnis and David S. McCaffrey, Jr., *Division of Petroleum Chemistry, 222nd ACS National Meeting, August 26-30, 2001*
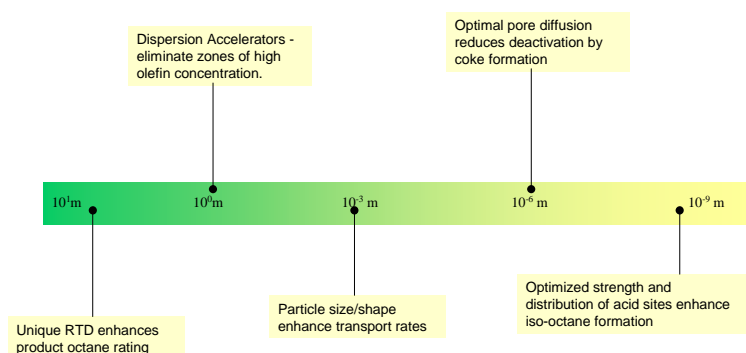
Figure 5. Innovations in the Exelus solid-acid catalyst alkylation technology

REMOVAL OF NITROGEN FROM LIQUID FUEL BY SUPERCRITICAL FLUIDS

Olubunmi M. Ogunsola

TEMEC, P.O. Box 1072, Woodbridge, VA 22195, USA

Introduction

The U.S. import of oil is projected to double, to about 20 million barrels/day, by 2025. At the same time, the U.S. resources of oil shale and tar sands are estimated at about 2 trillion barrels about 76 billion barrels, respectively. These huge unconventional oil resources are currently undeveloped (Dyni, 2000; OTA 1980 White Paper). Unfortunately, development of these unconventional domestic energy resources is limited due to several constraints which include the presence of nitrogen and sulfur, which can lead to increased emission of nitrogen oxides and sulfur dioxide, respectively if these impurities (nitrogen and sulfur) are not removed.

In order to obtain high value transportation fuels that will meet the new more stringent environmental requirements the sulfur and nitrogen have to be considerably reduced. Current conventional method of nitrogen and sulfur removal by hydro-treating is very expensive due to huge demand of expensive hydrogen for their effective removal. Supercritical fluids have been successfully used to break the carbon-nitrogen and carbon-sulfur bonds in model compounds by a number of researchers, including Ogunsola and Berkowitz (1995) and Ogunsola (1991, 2000). Since the nitrogen and sulfur contained in oil shale and tar sands are similar to these model compounds, supercritical fluids are, therefore, good candidates for removing nitrogen from shale oil and sulfur from tar sands-derived crude.

This paper presents the preliminary results of a study aimed at removing of nitrogen from shale oil by supercritical water (SCW).

Experimental

The raw oil shale sample was prepared by crushing it to less than 1.16mm and subsequently sieved. A -1.16mm +0.833mm size sample was then used for the experiment. Extraction of the oil shale sample was conducted in a one-liter stainless steel autoclave reactor system. Detailed description of the system is given elsewhere (Ogunsola, 1991). About 30 grams of prepared sample were used for each run. The extraction was done by using supercritical water at 400^oC and 450^oC at varying hot pressure of 14MPa, 17.5MPa and 21MPa. Liquid extracts from the samples were analyzed for elemental analysis (carbon, hydrogen, nitrogen, sulfur, and oxygen) and aromaticity. Conversion efficiency, defined as the fraction of organic carbon in the oil shale recovered oil (toluene-soluble), the

toluene-insoluble and THF-soluble fraction is considered to be the pre-asphaltene.

Results and Discussions

Table 1 below shows a summary of results obtained from this study.

Table 1. Summary of Results.

Temperature ^oC	400	450	400	450
Pressure, MPa	14	14	17.5	21
Conversion, %	35	22	30	32
Elemental Composition, %				
Carbon	76.8	77.0	79.2	80.4
Hydrogen	8.6	8.4	9.1	9.0
Nitrogen	1.1	1.3	1.3	1.5
Sulfur	9.97	12.4	8.3	6.4
Oxygen (by Difference)	3.5	0.9	2.2	2.7
H/C	1.34	1.31	1.38	1.35
^1H nmr, %				
H_{ar}	12.5	18.9	13.8	14.8
H_{ol}	0.0	0.0	0.0	0.0
H_n	7.6	6.6	5.1	7.8
Aromaticity, f_a	0.50	0.57	0.47	0.53

While it is obvious from the results on Table 1 that the carbon content of the liquid product increases with pressure at both temperatures, low temperature tends to favor hydrogenation of the oil. The aromaticity of the fuel could also be seen to be higher at higher temperature in this study. Extraction at low temperature appears to favor low nitrogen content of the fuel.

References

1. Congress of United States, Office of Technology Assessment: An Assessment of Oil Shale Technologies, June 1980 (OTA Report No. OTA-M-118)
2. Dyni, J. R. "Oil Shale" U. S. Geological Survey, February 2000.
3. Ogunsola, O.M. and Berkowitz, N. "Removal of Heterocyclic S and N from Oil Precursors by Supercritical Water" Fuel 74(10), p. 1485, 1995.
4. Ogunsola, O.M. "Decomposition of Isoquinoline and Quinoline by Supercritical Water" J. Hazardous Materials B74, p. 187, 2000.
5. Ogunsola, O.M. "Supercritical Water Extraction of Oil Shale" PhD Thesis, University of Alberta, Edmonton, Alberta, Canada, 1991.

STARTING DIESEL ENGINES AT LOW TEMPERATURES – IMPACT OF IGNITION QUALITY

Robert Freerks and *Joshua D. Taylor*[†]

*Syntroleum Corp., 4322 South 49th West Ave., Tulsa, OK 74107
[†] National Renewable Energy Laboratory, Golden, CO 80401

Introduction

The US EPA is promoting technologies to reduce idling time of heavy duty vehicles[1]. Individual states have promulgated regulations restricting idling to as short as 3 minutes in some cases[2]. The California Air Resources Board has begun to enforce its idling vehicle rule effective February 1, 2005[3]. Idle time reduction will significantly reduce non-productive fuel use and emissions. However, starting diesel engines that have cooled from normal operating temperature can lead to increased emissions. In addition, starting engines at temperatures near 0ºC can be difficult and lead to significant white smoke emissions due to unburned fuel until the engine warms sufficiently to combust all fuel injected into the combustion chamber. Fuel quality can directly impact both the ease of starting a diesel engine and the emissions produced during the warm-up phase of vehicle operation.

White smoke emissions from diesel engines occur during cold starting due to unburned hydrocarbons in the combustion chamber forming aerosols in the exhaust. Hara[4] et al. studied the impact of alkyl nitrates on cetane number, auto-ignition temperature, cold starting and white smoke emission from diesel engines during cold starting. They concluded that low cetane fuels result in longer times from cranking to steady idle speed at 25ºC start temperature, and that a 30 cetane number fuel will fail to start below 15ºC. For 50 cetane number fuel, starting deteriorated rapidly below 0ºC. However, white smoke emissions were not effected by adding a cetane improver, 2-ethylhexyl nitrate.

It is generally accepted that the high cetane number of Gas-to-Liquids (GTL) diesel fuel will improve startability at low temperatures, but little data exists to support this view. It is not known if GTL fuel will reduce white smoke and hydrocarbon emissions during and just after starting a diesel engine in cold climates. This report documents comparison of GTL diesel fuel versus conventional ASTM D975 No. 2-D and No. 1-D fuels at cold-start conditions.

Test Program

Ignition delay of numerous pure compounds and several diesel fuels of varying quality and source have been measured as a function of temperature (Figure 1) using the Ignition Quality Tester (IQT™) and reported previously[5]. Reactivity of different fuel molecules is postulated to be related to the reactivity of various sites in a molecule and the number of those reactive sites available to radical attack. In particular, the slope of the ignition delay versus temperature curves is related to the strength of the C-H bonds in the fuel molecules since the bond strength is correlated with the rate of H-abstraction reactions. These results show that the ignition delay at reduced temperatures is not only a function of cetane number, but also a function of the fuel molecular structure, which modifies the slope of the curve. We propose that the temperature at which the ignition delay reaches a certain value can be correlated with the minimum ambient temperature at which an engine will start using this fuel. This cold-start ignition delay is a separate fuel property that can be measured using the IQT™. This paper is an initial attempt to relate the low-temperature ignition delay to the minimum ambient starting temperature for an engine using GTL fuels.
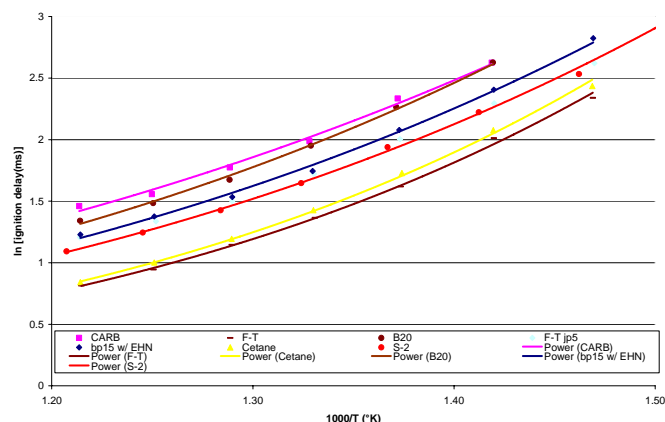

Figure 1. Arrhenius-type plot of fuel ignition delay data.

It is not well documented at this time how the compressed charge air temperature changes as ambient air temperature decreases,[§] or at what combustion chamber temperature cold start misfire and white smoke emissions occur. Therefore, there is a need for testing of starting ability of engines at low temperature in laboratory-controlled environments.

The impact of GTL fuel on diesel engine starting at low temperatures was investigated using a DDC Series 50 8.7 liter diesel engine. This program compared the performance of conventional No. 2 and No. 1 diesel fuels to Syntroleum S-2 Fischer-Tropsch GTL diesel fuel with respect to the ability of a diesel engine to start on a given fuel. No emissions measurements were made during these tests.

The fuel tested in this program was produced by Syntroleum at their Catoosa Demonstration Facility under a grant from the DOE. Syntroleum S-2 synthetic (GTL) diesel fuel is produced from natural gas using reforming technology to produce synthesis gas, which is fed to a Fischer-Tropsch reactor. S-2 is 100% paraffinic with both sulfur and aromatics below detectable limits. The fuel is composed primarily of normal and iso paraffins with an Iso/Normal ratio of 5:1. The fuel meets all ASTM D975 requirements and contains a complete additive package providing lubricity, corrosion, foam and oxidation performance. The cetane number of this fuel is above 74, which is the normal maximum calibration point for ASTM D613 Cetane Number measurements.

Tests were conducted as follows:
- Engine was flushed with test fuel and equilibrated at test temperature.
- Engine was cranked for 10 seconds or until starting occurred.
- If a start did not occur during a 10 second crank period, the engine was allowed to temperature equilibrate and cranking was again initiated two more times or until the engine started.

Starting performance of a fuel was deemed acceptable if it started during one of the three attempts at a temperature and at the next lower test temperature. If a start failure occurred at a temperature, the test temperature was dropped slightly and the test repeated to verify the start failure. For a limited temperature range, problematic starting was observed. Below some temperature, no amount of cranking resulted in a start condition. Figure 2 shows results for starting tests for the conventional No. 2-D fuel.

[§] A decrease in the intake charge air temperature of ~30-45°C results in a reduction of ~100-150°C in the compressed charge temperature assuming adiabatic compression.
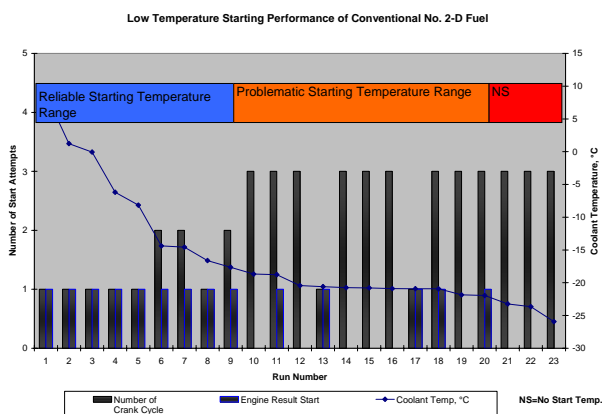
Figure 2. No. 2-D diesel fuel starting versus temperature.

Run number 9 in Figure 2 resulted in a start after two attempts at -18°C. Run number 10 resulted in a no-start after three attempts at -19°C. Below -22°C, no starting was observed.

No. 1-D diesel fuel performance is shown in Figure 3. This fuel started reliably down to -16°C and failed to start below -17°C. Although No. 1-D fuel has lower viscosity and lower cloud point than No. 2-D fuel, the ignitability of this fuel was not as good and therefore the startability was not as good as No. 2-D fuel.
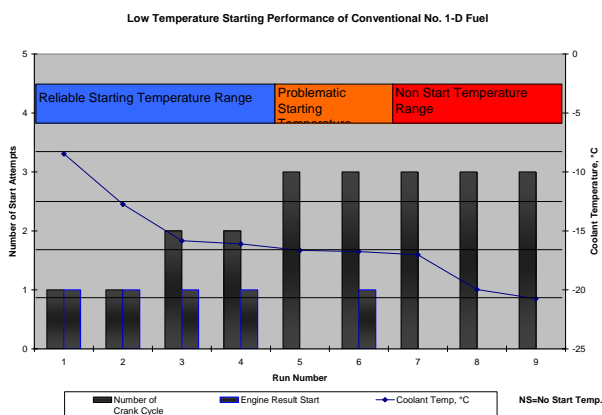

Figure 3. No. 1-D diesel fuel starting versus temperature.

Starting performance of S-2 is shown in Figure 4. Reliable starting was obtained down to -29°C with problematic performance down to -32°C. Below -32°C, no starting was observed.
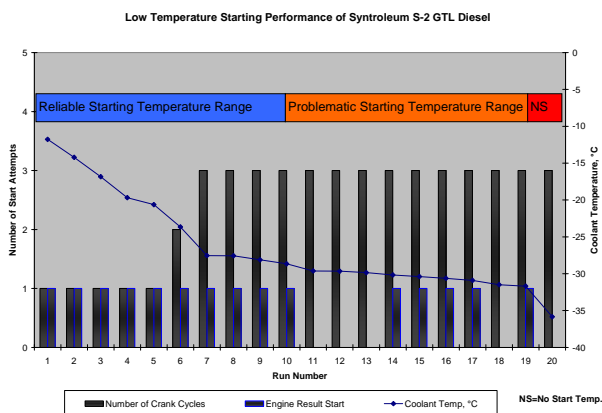

Figure 4. S-2 synthetic diesel fuel starting versus temperature.

Discussion and Conclusions

GTL diesel fuel with high cetane allows reliable starting of diesel engines at 11°C lower ambient temperatures than conventional No. 2-D fuel. This 11°C difference in ambient air temperature would result in a difference of compressed charge temperature of ~33°C (assuming adiabatic compression). If we assume that the minimum ambient temperature at which the engine will start is correlated with the temperature at which the ignition delay is a certain value, we can relate the engine data (Figures 2-4) with the IQT™ data shown in Figure 1.

For example, if we assume a critical cold-start ignition delay of 6 ms, then the S-2 charge temperature would be 468°C (from Figure 1) and the 2-D charge temperature would be 502°C. This shows a 34°C difference, which agrees well with the difference in charge temperature we would expect from the adiabatic compression.

This data just begins to explain the real world performance of different fuels in engines under cold start conditions. Emissions measurements and additional performance data at cold temperatures is needed. The DOD RDECOM will be conducting a series of tests on synthetic F-T derived JP-8 fuel and blends utilizing engines of interest to the US Army later this year[6].

References
(1) Levinson, T. National Idling Reduction Network News, **2005**. http://www.eere.energy.gov/vehiclesandfuels/pdfs/newsletters/feb05_network_news.pdf
(2) American Transportation Research Institute, Compendium of Idling Regulation, **2004**. http://www.atri-online.org/research/results/idling_chart.pdf
(3) California EPA ARB News Release 05-04, ARB Begins Enforcement of Idling Vehicle Rule, January 31, 2005. http://www.arb.ca.gov/newsrel/nr013105.htm
(4) Hara H., Itoh Y., Henein H. A. and Bryzik W. "Effect of Cetane Number with and without Additive on Cold Startability and White Smoke Emissions in a Diesel Engine", *SAE,* **1999**-0101476.
(5) Taylor, J. D.; McCormick, R. L. *Prepr. Pap.-Am. Chem. Soc.*, *Div. Fuel Chem.*, **2005**, *50* (1), 325.
(6) Personal communications with Pat Muzzell, US Army RDECOM, April 2005

CRYPTOMELANE AS HIGH CAPACITY SULFUR DIOXIDE ABSORBENT FOR DIESEL EMISSION CONTROL

Liyu Li and David L King

Materials Division, Pacific Northwest National Laboratory
P.O. Box 999, Richland, WA 99354

Introduction

Cryptomelane, $K_xMn_8O_{16}$, has been identified as a high capacity sulfur oxide absorbent under oxidizing and inert conditions.[1] Cryptomelane can be synthesized either from a mixture of $KMnO_4$ and $MnSO_4$ or a mixture of $MnSO_4$ and KOH.[2] Under oxidizing conditions, cryptomelane synthesized from $KMnO_4$ and $MnSO_4$ is stable up to 600°C, and cryptomelane synthesized from $MnSO_4$ and KOH is stable up to 800°C. Over a temperature range from 250°C to 475°C, cryptomelane SO_2 capacity can be as high as 70 wt%, which is almost ten times as high as that of conventional metal oxide-based SO_2 absorbents. The dominant mechanism for SO_2 absorption by cryptomelane is through the oxidation of SO_2 to SO_3 by Mn^{4+} and Mn^{3+} followed by SO_3 reaction with Mn^{2+} to form $MnSO_4$.

In this presentation, we describe a study of the stability of cryptomelane under reducing conditions and lean-rich cycling conditions that simulate the proposed NO_x trap aftertreatment system.[3] It has been found that although the cryptomelane materials are not stable under most reducing conditions, the reduced form can be oxidized back to the original cryptomelane structure. Cryptomelane which has experienced lean-rich cycles up to 550°C still has very high SO_2 capacity.

Experimental Section

Cryptomelane was synthesized either from a mixture of $KMnO_4$ and $MnSO_4$ or a mixture of $MnSO_4$ and KOH.[2] The adsorbents were evaluated mostly as 40-80 mesh granules, formed by pressing a tablet at 20,000 psi for 5 minutes followed by crushing and screening.

A large portion of the stability study was carried out using a Netzsch STA 409 Thermogravimetric Analysis (TGA)-Differential Scanning Calorimetry (DSC)-Mass Spectroscopy (MS) system. Different gases, including air, 2% H_2 in Ar, 2% C_3H_6 (propylene) in Ar, and He were used for the TGA-DSC-MS analysis. To get a large amount of treated samples for other characterizations, cryptomelane was also treated in a tube furnace with flowing air, 2% C_3H_6 in Ar, simulated rich condition diesel engine exhaust, and simulated lean condition diesel engine exhaust. Lean-rich cycling treatments were carried out with an AMI-200R-HP unit (Altamira Instruments, Pittsburgh, PA), which can automatically switch the feed to a heated reactor between lean and rich exhaust gases at given time intervals. The composition of these simulated exhausts is given in **Table 1** below. Two samples were prepared for us by Caterpillar Inc. for

subsequent testing and analysis. The exhaust compositions of those treatments are identified as "Lean Condition" and "Rich Condition" in **Table 1**. The two different feed compositions for lean-rich cycling experiments carried out in our laboratory are identified as "Lean-rich cycle A" and "Lean-rich cycle B".

Powder X-ray diffraction (XRD), BET surface area (SA), and scanning electron microscopy (SEM) images were collected on some of the tested materials. The SO_2-absorption tests were performed in a small fixed bed quartz tube reactor, which was heated by a small clam-shell furnace. Reactant gases were metered using mass flow controllers. The SO_2 analytical system comprised a HP6890 gas chromatograph equipped with a Sulfur Chemiluminescent Detector (SCD), which has been described in detail previously.[4] During the experimental run the analytical system operated continuously, sampling the effluent every three minutes. The minimum detection limit of the system to SO_2 is approximately 50 ppb. Typical measurements employed a 0.2 g 40-80 mesh particle sample. The standard absorption tests were performed at 325°C, using a feed gas of 250 ppm SO_2 in air, at a flow of 8,000 hr^{-1} gas hourly space velocity (GHSV).

Results and Discussion

Stability under oxidizing conditions. Two additional tests were performed to further check the stability in an oxidizing atmosphere. In the first test, cryptomelane prepared by the $MnSO_4$ oxidation method was treated at 600°C for 3 hr in air containing 10% H_2O, to test for steam/air stability. In the second test, cryptomelane prepared by the reflux method was treated at 500°C for 1 hr in simulated lean exhaust gas ("Lean Condition" in **Table 1**). Following these treatments, no structural changes were observed based on XRD analysis. The SO_2 capacities were measured following these two treatments. Even after these extreme conditions, cryptomelane still has more than 45 wt% SO_2 breakthrough capacity.

Stability under inert atmosphere. Cryptomelane shows high SO_2 capacity at 325°C under an inert atmosphere.[1] Its stability under ultra high purity helium was studied using TGA-DSC-MS. Under inert atmosphere, cryptomelane from the reflux method is stable up to 450°C, and cryptomelane from the $MnSO_4$ oxidation method is stable up to 580°C. At higher temperatures, cryptomelane decomposes. In general, cryptomelane is less stable under inert conditions than under air.

Stability under reducing conditions. As a high valence manganese oxide, cryptomelane is unstable under reducing conditions. **Figures 1(a)** shows the DSC analysis results of cryptomelane under 2% C_3H_6 in Ar. Cryptomelane is reduced at as low as 300°C. After reduction, Mn_3O_4 and MnO form. Mn_3O_4 is further reduced to MnO when the reduction temperature is higher than 550°C. A similar result was also obtained with 2% H_2 in Ar as reductant. Cryptomelane from the $MnSO_4$ oxidation synthesis method shows similar results.

Table 1. Composition of simulated diesel engine exhausts used in the study

Simulated Exhaust		Carbon Soot	CO	CO$_2$	C$_3$H$_6$	H$_2$	H$_2$O	SO$_2$	O$_2$	NO$_2$	NO	N$_2$
Lean Condition		5x10^{-5} g/L	3250 ppm	7.1%	360 ppm	--	--	--	10.2%	--	230 ppm	Balance
Rich Condition		2x10^{-5} g/L	2000 ppm	10%	1000 ppm	--	10%	--	0~1%	--	500 ppm	Balance
Lean-rich cycle A	Lean	--	--	10%	--	--	10%	--	12%	--	500 ppm	Balance
	Rich	--	4%	10%	4000 ppm	1.3%	10%	--	1.5%	--	500 ppm	Balance
Lean-rich cycle B	Lean	--	--	5%	--	--	--	5.15 ppm	12%	20 ppm	180 ppm	Balance
	Rich	--	2%	12.5%	333 ppm	2%	--	--	--	--	--	Balance

The MnO from reduced cryptomelane can be easily oxidized upon heating in an oxidizing atmosphere. **Figure 1 (b)** gives the DSC trace upon re-oxidation of the MnO product obtained by initial cryptomelane reduction in 2% C_3H_6 in He at 550^oC. As can be seen, the MnO can be re-oxidized as low as 250^oC. After oxidation at 500^oC for 1hr, most of the reduced cryptomelane recovers the original cryptomelane crystal structure, as shown in **Figure 2**. The minority product of re-oxidation is Mn_3O_4.
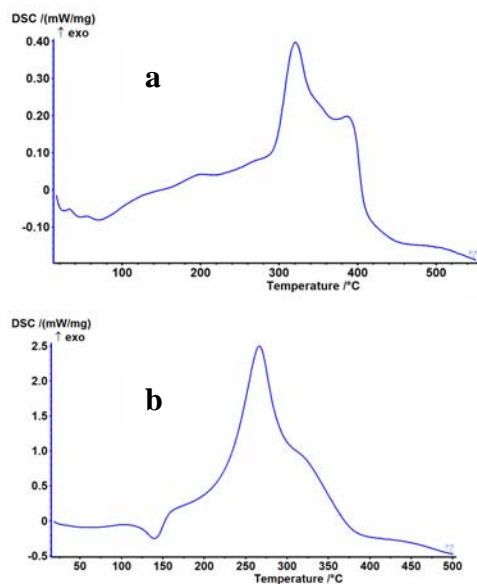

Figure 1. a: DSC trace of cryptomelane in 2% C_3H_6. Test condition: 10^oC /min heating rate, 2% C_3H_6 in Ar at 40 ml/min flow; b**:** DSC trace of 550^oC, 2% C_3H_6 treated-cryptomelane heated in air. Test condition: 10^oC/min, air at 40 ml/min.
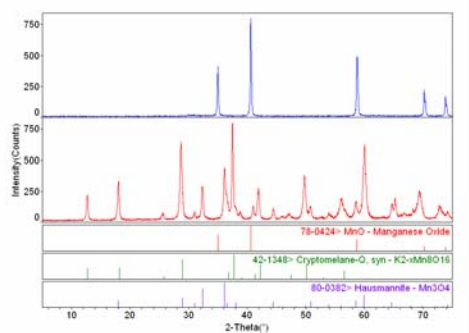

Figure 2. XRD patterns of reduced (top) and re-oxidized (bottom) cryptomelane. Reduction: in 2% C_3H_6 at 550^oC for 1 hr; Re-oxidation: in air at 500^oC for 1 hr

Stability under lean-rich cycling. To study the effect on cryptomelane of the lean-rich cycling protocols that have been proposed for NO_x traps, a cryptomelane sample was treated under simulated lean-rich cycles at 475^oC for 6.5 hours (cycling at 6 minutes lean and 30 seconds rich). The exhaust composition was given in **Table 1** (lean-rich cycle A). Both lean and rich exhaust gas flowed at 26,000 hr^{-1} GHSV through cryptomelane.

Almost identical XRD patterns were obtained of the cryptomelane samples before and after the lean-rich treatment. Some morphology changes were observed under SEM, and the BET surface area decreased from 74 m^2/g to 20 m^2/g after treatment. **Figure 3**

shows the SO_2 absorption performance of the lean-rich treated cryptomelane, which is close to that of the fresh absorbent. This indicates that the SO_2 absorption capacity of cryptomelane is not simply a function of its surface area.

NO_x traps may be required to operate over a temperature range 250^oC to 550^oC, therefore the SO_x trap should also operate stably over this same range. Subsequent experiments exposed cryptomelane to lean-rich cycling at 250^oC, 400^oC, and 550^oC. Each treatment lasted 6 hours, with the cycling protocol 4 minutes lean (50,000 hr^{-1} GHSV) and 20 seconds rich (10,000 hr^{-1} GHSV). The lean and rich gases composition is given in **Table 1** (lean-rich cycle B). After 6 hours of lean-rich treatments all three samples give very high SO_2 capacities (> 45 wt%).

No structural changes were observed with cryptomelane from the reflux method after 250^oC and 400^oC lean-rich treatment. However, after 550^oC treatment, cryptomelane from the reflux method was mostly reduced to Mn_2O_3, whereas cryptomelane from the $MnSO_4$ oxidation method only showed slight structure change after the same lean-rich treatment. The XRD analysis indicates that cryptomelane prepared by the $MnSO_4$ oxidation method is more stable toward lean-rich cycling than cryptomelane prepared by the reflux method.
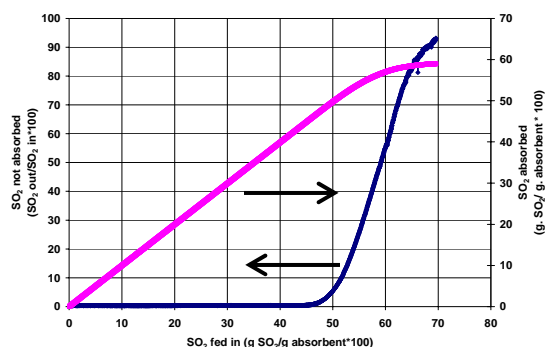

Figure 3. SO_2 absorption of lean-rich treated cryptomelane.

Treatment condition: 475^oC for 6.5 hr, cycling at 6 min lean and 30s rich, lean and rich gas flows at 26,000 hr^{-1} GHSV. Lean and rich gas composition (A) is given **Table 1**. Test conditions: 325^oC, 250 ppm SO_2 in air at 8,000 hr^{-1} GHSV

Stability of SO_2 -loaded absorbent. After SO_2 absorption on cryptomelane, $MnSO_4$ and K_2Mn_2 $(SO_4)_3$ form. These phases are stable up to 700^oC under an oxidizing atmosphere. The stability of SO_2-saturated cryptomelane under reducing conditions was studied using TGA-MS. In terms of sulfur retention, spent cryptomelane is stable up to 600^oC in 2% H_2 in He. Above 600^oC, SO_2 and H_2S are released.

References
1. Li, L., King, D.L., *Ind. Eng. Chem. Res.* **2005**, *44*, 168.
2. DeGuzman, R.N., Shen, Y.F., Neth, E,J., Suib, S.L., O'Young, C.K., Levine,S., Newsam, J.M., *Chem. Mater.* **1994, 6, 815.**
3. Takahashi, N., Shinjoh, H., Iijima, T., Suzuki, T., Yamazaki, K., Yokota, K., Suzuki, H., Miyoshi, N., Matsumoto, S.I., Tanizawa, T., Tanaka, T., Tateishi, S.S., Kasahara, K., *Catal. Today* **1996**, *27*, 63.
4. Li, L., King, D.L., *Ind. Eng. Chem. Res.* **2004**, *43*, 4452.

ADSORPTION PROPERTIES CHANGE OF Ni/Y ON SULFUR COMPOUNDS DEPENDING ON THE DIESEL COMPOSITION

Chang Hyun Ko, Vinay M. Bhandari, Jung Geun Park, Jong-Nam Kim, Sang Sup Han, Soon Haeng Cho

Separation Process Research Center, Korea Institute of Energy Research, 71-2, Jang-dong, Yu-sung-gu, Daejeon, Korea, 305-343

Introduction

The demand on clean transportation fuel has increased due to the strict regulation to protect environment or fuel cell application. Especially, fuel cell needs extremely low level sulfur concentration fuel because even small amount of sulfur can cause deactivation of catalyst in reformer. However, decrease of sulfur concentration in transportation fuel from 300 ppmw to less than 1 ppm by hydrodesulfurization (HDS) process, already applied in refinery plant, was extremely difficult due to the low reactivity of HDS catalysts for refractory sulfur compounds, which have steric hindrance such as benzothiophene (BT), dibenzothiophene (DBT) and 4,6-dimethyldibenzothiophene (4,6-DMDBT) [1].

Recently, Yang and co-workers introduced a new class of sulfur removal method in transportation fuel: removal of sulfur compounds in diesel at ambient temperature using sulfur selective adsorbents[2]. They reported that various kinds of metal-ion exchanged Y zeolites, such as Ni/Y, Cu/Y and so on, showed remarkably high capacity and selectivity for refractory sulfur compounds in commercial diesel[3-5]. They proposed that π-complexation bonding between sulfur compounds and metal cation exchanged inside the pores of Y zeolite impose such selectivity and capacity on zeolite based adsorbents[2,6]. However, no systematic study on sulfur compound adsorption has been reported yet.

For more understanding on this selective adsorption phenomenon, we investigated the adsorption properties of Ni/Y on BT, DBT and 4,6-DMDBT in model diesel. The model diesel contained 50 ppm BT, 50 ppm DBT and 50 ppm 4,6-DMDBT in n-octane. The capacity of Ni/Y was very high: 40 mg S/g. However, the capacity decreased drastically as soon as the presence of aromatics and moisture. We also compared the adsorption behavior of Ni/Y in model diesel with that in commercial diesel.

Experimental

Adsorbent preparation. Na-Y zeolite was obtained from Aldrich (Si/Al = 2.37). Ni/Y was prepared using liquid phase ion exchange method at room temperature. 1.0 g of Na-Y was stirred in 1 M nickel nitrate solution for 8-10 hours and then washed with deionized water to remove the excess nickel salt solution. The ion exchange process was repeated 3 times and each process time was more than 3 hours to ensure complete exchange of nickel ion instead of sodium ion. The ion exchange was carried out at room temperature and at pH ~5. After ion exchange and washing, the adsorbent was dried in vacuum at 298 K to remove the moisture. The dried sample was stored in air-tight bottles, kept in desiccators. Appropriate particle size (125 ~ 600 um) was obtained by sieving for breakthrough test to reduce pressure drop and maximize effluent contact time on adsorbent.

Reagents and standards. The refractory sulfur compounds vis. BT (95%), DBT (98%) and 4,6-DMDBT (97%) were used as-received from Aldrich without further purification. We chose n-octane (99%) as a solvent in model diesel and obtained from Junsei. A sample of commercial diesel was obtained from a gas-station in Daejeon, South Korea.

Breakthrough Test: Fixed bed adsorption. Breakthrough tests were carried out in quartz tubes, having inside diameter of 4 mm and outside diameter of 6 nm, with tube length of 300 mm. The experimental set-up consisted of a constant flow liquid flow pump, vertical glass column and feed solution bottles. Upflow conditions were used in all the experiments. The activation of Ni/Y was carried out using the procedures recommended by Yang and co-workers. The Ni/Y was heated from ambient temperature to 623 K for 3 hours and then maintained 623 K for 18 hours in helium gas atmosphere. The helium gas was initially passed through a column of 3A molecular sieves to remove moisture, if any, before passing through the adsorbent to remove moisture contamination after activation process. Ni/Y was green after ion exchange, but became pinkish color after proper activation treatment.

Sulfur Concentration Analysis. All the samples were analyzed using HP 6890 series gas chromatograph, equipped with SUPELCO 24158 SPB-1 SULFUR capillary column and a flame photometric detector (FPD). Identification of BT, DBT and 4,6-DMDBT was carried out using the standard solutions. We obtained relationship between peak area and sulfur concentration of each sulfur compound. We measured peak area of unknown sample by GC-FPD, then calculated the sulfur concentration based on this relationship.

Results and Discussion

Figure 1 showed the breakthrough curves of Ni/Y for model diesel, consisted of 50 ppm BT, 50 ppm DBT, 50 ppm 4,6-DMDBT in n-octane. A flow rate of 0.4 ml/min was used in this experiment. Ni/Y can purifie about 300 ml of 150 ppmw model diesel. The volume of purified model diesel means that sulfur adsorption capacity of Ni/Y calculated was about 40 mg S/g ads. The breakthrough point can be estimated by observing the development of color front in adsorbent. The pinkish color changed to brown color after breakthrough.

Figure 1 also indicated an interesting selectivity patterns. Firstly, BT was found to elute. Secondly, 4,6-DMDBT eluted. Finally, DBT came out from the Ni/Y adsorbent. This suggests that the selectivity of Ni/Y on refractory sulfur compound was DBT > 4,6-DMDBT > DBT.
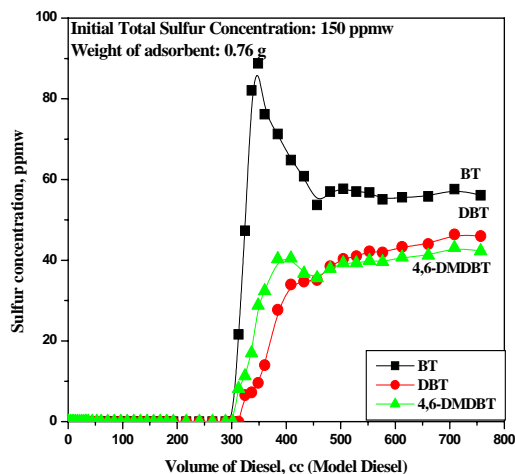

Figure 1. The breakthrough curves of refractory sulfur compounds for Ni/Y in model diesel.

Based on model diesel breakthrough test using sulfur compounds and n-octane solvent, Ni/Y had expected to be a

promising adsorbent for adsorptive sulfur removal in transportation fuel. To confirm this possibility, Ni/Y was applied for the purification of commercial diesel by breakthrough test. The flow rate was 0.2 ml/min and activation time to maintain 623 K was 10 hours. However, Figure 2 showed the drastic decrease in purification volume of commercial diesel compared to that of model diesel. As we used the same types of adsorbent, Ni/Y, the only difference in this experiment was the composition of the effluents: model diesel and commercial diesel. The decrease of adsorption capacity of Ni/Y for commercial diesel might be affected by the diesel composition.
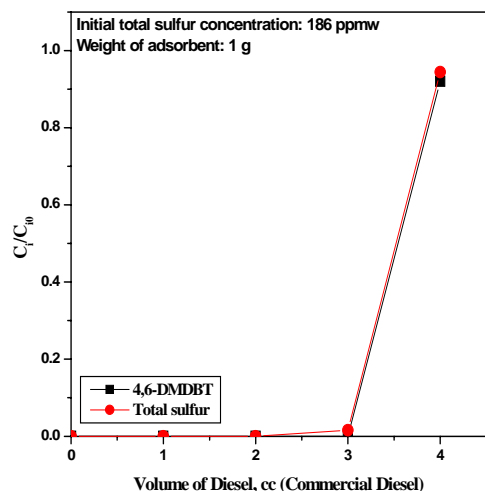

Figure 2. The breakthrough of refractory sulfur compound on Ni/Y using commercial diesel
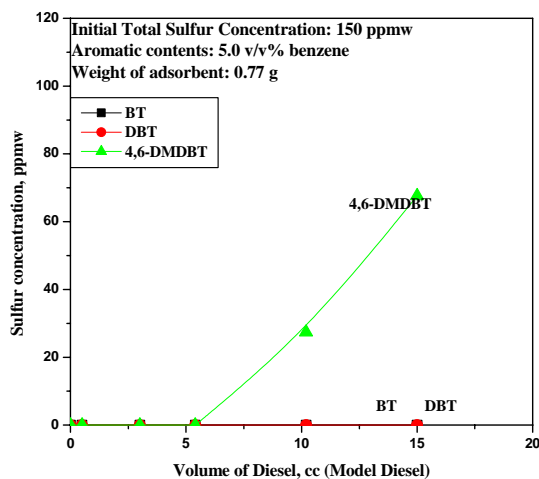

Figure 3. The breakthrough curve for sulfur compound on Ni/Y using model diesel after addition of 5 wt% benzene

Figure 3 showed the lowering of sulfur adsorption capacity after addition of benzene on model diesel. Ni/Y was able to treated 300 ml of pure model diesel, but Ni/Y was only able to purify less than 6 ml of 5 v/v % benzene added model diesel. As the only difference in both effluents was benzene composition, we were able to attribute

adsorption capacity decrease to the presence of benzene in model diesel. In view of the fact that commercial diesel has a wide range for the aromatic content (15 ~ 47%), higher aromatics in commercial diesel could be one possible reason for the lower capacity.

We also examined the effect of moisture on Ni/Y for sulfur compound adsorption because moisture was one of the most frequently appeared species among various contaminating ones.
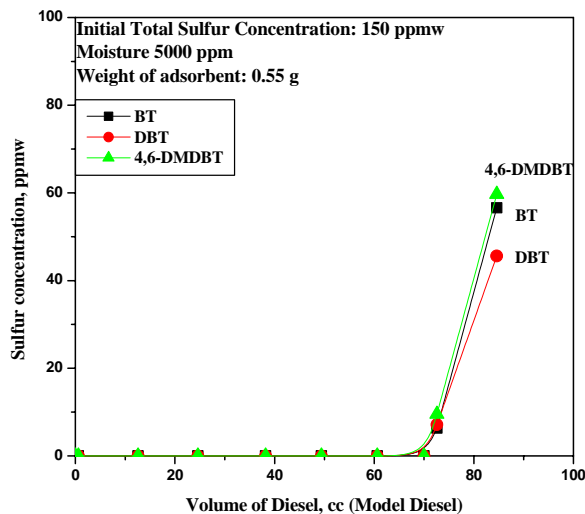

Figure 4. The moisture effect on the Ni/Y adsorption on sulfur compound

As shown in Figure 4, 0.5 wt% moisture reduced more than 60% of adsorption capacity. Thus, pre-treatment of moisture prior to adsorptive sulfur removal in commercial diesel might be an essential process to ensure the reliability and reproducibility of adsorptive desulfurization process.

Conclusion
We investigated the adsorption properties of Ni/Y on refractory sulfur compounds in model diesel by breakthrough test. Apart from high adsorption capacity on sulfur compounds in model diesel, adsorption capacity of Ni/Y decreased drastically due to the presence of aromatics and moisture.

References
(1) Yang, R. T. In *Adsorbents: Fundamentals and Applications* and references there in; Wiley: New York, 2003; chap. 10
(2) Yang, R. T.; Hernandez-Maldonado, A. J.; Yang, F. H. *Science* **2003**, *301*, 79.
(3) Hernandez-Maldonado, A. J.; Yang, R. T. *Ind. Eng. Chem. Res.* **2003**, *42*, 3103.
(4) Hernandez-Maldonado, A. J.; Yang, R. T. *Ind. Eng. Chem. Res.* **2004**, *43*, 1081.
(5) Hernandez-Maldonado, A. J.; Yang, R. T. *AIChE J.* **2004**, *50*, 791.
(6) Hernandez-Maldonado, A. J.; Yang, R. T. *J. Am. Chem. Soc.* **2004**, *126*, 992.

EFFECT OF HIGH SURFACE AREA SILICEOUS SUPPORTS ON THE STRUCTURE AND CATALYTIC PERFORMANCE OF Ni₂P CATALYSTS

Yong-Kul Lee and S. Ted Oyama

Environmental Catalysis and Nanomaterials Laboratory, Department of Chemical Engineering, Virginia Tech, Blacksburg, VA 24061

Introduction

Environmental regulations for reducing motor vehicle emissions has put considerable pressure on the refining industry worldwide to produce cleaner fuels, and has motivated much research for the development of new hydrotreating catalysts. Among alternatives to the widely used sulfides are transition-metal carbides, nitrides, and phosphides (1,2,3,4). Metal phosphides are a novel catalyst group for deep hydrotreating and have received much attention due to their high activity for hydrodesulfurization (HDS) and hydrodenitrogenation (HDN) of petroleum feedstocks (4,5,6,8). Previous studies of silica-supported Ni₂P employed a low surface area (90 m² g⁻¹) support (6,7). It is the objective of this work to investigate a mesoporous siliceous material (790 m² g⁻¹) as support. Particular attention is placed on understanding the effect of nitrogen, sulfur and aromatic compounds on the catalytic behavior, as these compounds are reported to inhibit HDS. The present study also includes the use of X-ray absorption fine structure (XAFS) spectroscopy to study the structure of the finely dispersed phosphide phases before and after reaction. As will be shown the samples after use show evidence for the formation of a surface phospho-sulfide phase of very high activity.

Experimental

Commercial SiO₂ supports (Cabot, Cab-O-Sil) of low surface area (L-90, 90 m² g⁻¹) was used as received. A mesoporous MCM-41 silica support was synthesized following a literature procedure (9). The supported Ni₂P catalysts were prepared with excess phosphorus (Ni/P=1/2) and a loading of 1.16 mmol Ni/g support (12.2 wt.% Ni₂P/SiO₂). Previous studies (6,7) had shown that this composition and loading level gave high activity and stability in hydroprocessing reactions. Samples prepared with low surface area silica (L90) were denoted as Ni₂P/SiO₂-L. The synthesis of the catalyst involved two steps (4,6,7). In the first step, a supported nickel phosphate precursor was prepared by incipient wetness impregnation of a solution of nickel nitrate and ammonium phosphate, followed by calcination at 673 K. In the second step, the supported metal phosphate was reduced to a phosphide by temperature-programmed reduction (TPR). In catalyst preparation, larger batches using up to 5.50 g of supported nickel phosphate were prepared in a similar manner by reduction to 873 K and 893 K for Ni₂P/SiO₂-L and Ni₂P/MCM-41, respectively. Sulfided Ni-Mo/Al₂O₃ (CR 424) was used as reference.

The prepared catalysts were characterized by XRD, N₂ adsorption and CO chemisorption. Also, X-ray absorption (XAS) spectra at the Ni K edge (8.333 keV) of reference and catalyst samples were recorded in the energy range 8.233 to 9.283 keV using synchrotron radiation at the National Synchrotron Light Source (NSLS) at Brookhaven National Laboratory (BNL), beamline X18B.

Hydrotreating was carried out at 3.1 MPa (450 psig) at two different temperatures, 573 K (300 °C) and 613 K (340 °C) in a three-phase upflow fixed-bed reactor. The feed liquid was prepared by combining different quantities of tetralin (Aldrich, 99%), n-tridecane (Alfa Aesar, 99%), quinoline (Aldrich, 99%), 4,6-dimethyldibenzo-thiophene (4,6-DMDBT, Fisher, 95%), dimethyldisulfide (DMDS, Aldrich, 99%), and n-octane (Aldrich, 99%).

Results and Discussion

Figure 1 shows the hexagonal structure of Ni₂P. The Ni₂P unit cell has two types of Ni and P sites (denoted as Ni(I), Ni(II) and P(I), P(II)), which form two different trigonal prisms in Ni₂P consisting of various Ni-P and Ni-Ni subshells.

Figure 1. Local structure of Ni₂P with two types of trigonal prisms.

Figure 2 shows the Fourier transforms of the Ni K-edge EXAFS spectra for the freshly prepared samples before reaction and a bulk reference Ni₂P sample. For the bulk Ni₂P the Fourier transform gives two main peaks, a smaller peak at 0.171 nm, and a larger peak at 0.228 nm. For the supported Ni₂P samples there are also two main peaks located at almost the same positions as those of the bulk Ni₂P reference, but with the larger peak weakened and broadened as the surface area of the support increases.
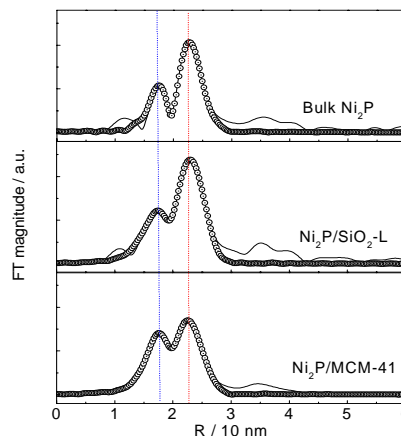

Figure 2. EXAFS analysis results for the fresh samples. The solid lines are the experimental curves and the circles are calculated points.

EXAFS analysis is particularly useful for characterizing the highly dispersed phase on the supports with large surface area. The Feff simulation allowed the assignment of those peaks that appeared in the Fourier transform. The first small peak centered at 0.180 nm was due to P neighbors at 0.2209 and 0.2266 nm and the second larger peak centered at 0.230 nm was due to a mixed feature of P neighbors at 0.2369 and 0.2457 nm and of Ni neighbors at 0.26783 nm. For the curve fittings the three dominant shells of two Ni-P shells at 0.2266 and 0.2456 nm and one Ni-Ni shell at 0.2678 nm were selected from the simulation results and used as references for phase shift and amplitude calculations. These give reasonable parameters for all samples (Table 1). For example, fitting for the bulk Ni₂P gives 2 P neighbors at 0.2253 nm and 1.75 P neighbors at 0.2401 nm and 3.99 Ni neighbors at 0.2644 nm. In contrast to bulk Ni₂P, for the supported Ni₂P samples the coordination number of the second shell, Ni-P at 0.2456 nm, increases as dispersion increases, even though the Ni-P bond length decreases. Interestingly, the bond length for the Ni-Ni shell increases with the coordination number as the dispersion increases. It is thus likely that the more dispersed

Ni$_2$P catalyst contains more P atoms, and that the interstitial P atoms lengthen the distance between Ni atoms and weaken the Ni-Ni bond. Ni$_2$P/MCM-41 containing highly dispersed Ni$_2$P particles underwent less loss in P, even after the high temperature reduction. This suggests that the smaller particles have a stronger interaction between the Ni and P atoms.
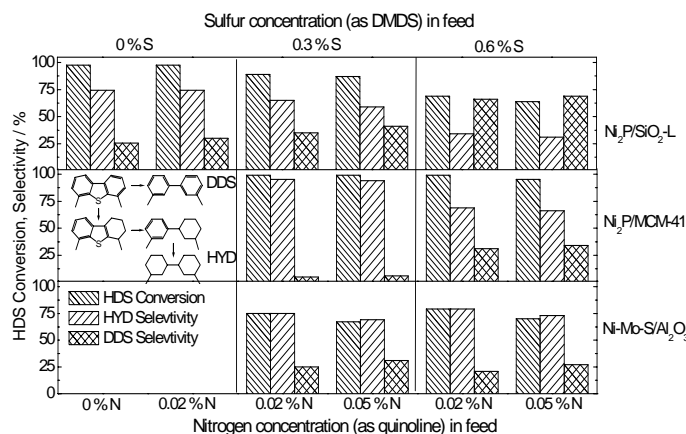

Figure 3. Comparison of hydrogenation/dehydrogenation activity for 4,6-DMDBT over Ni$_2$P/ SiO$_2$-L, Ni$_2$P/ MCM-41 and Ni-MoS/Al$_2$O$_3$.

Figure 3 compares the conversion and the product selectivities toward direct desulfurization (DDS) and hydrogenation (HYD) of 4,6-DMDBT as a function of nitrogen (as quinoline) and sulfur (as DMDS) content in the feed for the catalysts at 613 K and 3.1 MPa. The catalytic activity for the catalyst samples in HDS of 4,6-DMDBT followed the order, Ni-MoS/Al$_2$O$_3$ < Ni$_2$P/SiO$_2$-L < Ni$_2$P/MCM-41 under 0.35 % S, 0.02 % N, and 1% tetralin. The Ni$_2$P/MCM-41 showed much better resistance to the inhibition of S and N-compounds with maintenance of higher HDS conversion compared to Ni$_2$P/SiO$_2$-L. The EXAFS analysis confirms that the Ni-Ni bond length is widened with dispersion and this feature comes with an increase in Ni-P coordination and a decrease in Ni-P bond length. Thus the higher resistance to the sulfidation can be explained by the stronger interaction between Ni and P species for the highly dispersed Ni$_2$P catalysts. These results thus suggest that the HDS

activity and the resistance to S and N-compound highly depend on the dispersion of the Ni$_2$P phase.

Conclusions

Nickel phosphide (Ni$_2$P) catalysts supported on silica and MCM-41 showed high HDS activity for 4,6-DMDBT compared to a commercial Ni-Mo-S/Al$_2$O$_3$ catalyst at 573 K (300 ^{o}C) and 613 K (340 ^{o}C) and 3.1 MPa based on equal sites (70 μmol) loaded in the reactor. The desulfurization was dominated by the hydrogenation pathway over the Ni$_2$P catalysts and showed less inhibition by S and N-compounds compared to the sulfide catalysts. Selectivity and performance was higher on the more dispersed catalysts in the order Ni$_2$P/MCM-41 > Ni$_2$P/SiO$_2$-L and this is attributed to the increase in the number of and quality of active sites. Smaller Ni$_2$P particles have better resistance to S and N compounds due to the stronger interaction between Ni and P in the dispersed Ni$_2$P phase. EXAFS line shape analysis indicates the formation of a phospho sulfide phase which is favored for the catalysts with shorter Ni-Ni bond length particularly under high S in feed and at relatively high temperature. The phase is responsible for the high activity of the nickel phosphide catalysts.

References
(1) Schlatter, J. C.; Oyama, S. T;. Metcalfe, J. E. ; and Lambert, J. M. *Ind. Eng. Chem. Res*., **1988**, *27*, 1648.
(2) Oyama, S. T. (Ed.), The Chemistry of Transition Metal Carbides and Nitrides; Blackie Academic and Professional: London, 1996.
(3) Robinson, W. R. A. M.; van Gastel, J. N. M.; Korányi, T. I.; Eijsbouts, S. ; van Veen, J. A. R. ; and de Beer, V. H. J., *J. Catal.* **1996**, *161*, 539.
(4) Li, W.; Dhandapani, B.; and Oyama, S. T., *Chem. Lett*. **1998**, 207.
(5) Stinner, C.; Prins, R.; and Weber, Th., *J. Catal.* **2000**, *191*, 438.
(6) Oyama, S. T.; Wang, X.; Lee, Y.-K.; and Requejo, F. G., *J. Catal.* **2002**, *210*, 207.
(7) Oyama, S. T.; Wang, X.; Lee, Y.-K.; and Chun, W.-J., *J. Catal.* **2004**, *221*, 263.
(8) Oyama, S. T., *J. Catal.* **2003**, *216*, 343.
(9) Cheng, C.-F.; Park, D. H.; and Klinowski, J., *J.Chem. Soc., Faraday Trans.*, **1997**, *93(1)*, 193.

Table 1. Line-Shape Analysis of EXAFS Spectra and Physical Properties of the Supported Ni$_2$P Catalysts

Samples	Ni-P						Ni-Ni (I, II)			R (%)	CO uptake / μmol g^{-1}	BET surface area / m^2 g^{-1}
	Ni-P (I)			Ni-P (II)								
	CN	R	σ^2	CN	R	σ^2	CN	R	σ^2			
Ni$_2$P Feff reference	2	0.2266		1	0.2369		4	0.2678				
Ni$_2$P (bulk)	2.0	0.2253	3.00	1.7	0.2401	0.499	3.99	0.2644	6.00	0.48	-	-
Ni$_2$P / SiO$_2$-L	1.99	0.2234	4.900	2.6	0.2399	6.352	3.43	0.2612	8.001	0.96	25	88
Ni$_2$P / MCM-41	1.99	0.2210	2.884	3.5	0.2375	4.361	2.88	0.2631	8.477	1.24	41	487

ΔR filtered = 0.1427 - 0.27598 nm, S$_o^2$ = 0.9, CN: coordination number, R: bond distance (/nm), σ^2: Debye-Waller factor (/10^{-5} nm^2)

IMPROVING ENZYMATIC TRANSFORMATION OF WASTE EDIBLE OIL TO BIODIESEL BY ADDING ORGANIC BASE

Zhi-feng Chen, Ming-hua Zong*, Hong Wu

Biotechnology Department, South China University of Technology, Guangzhou 510640, P.R.China
*Author for correspondence (Fax: 86-20-22236669; E-mail: btmhzong@scut.edu.cn)

Introduction

Wastes edible oil, originated from restaurants and household disposals, is creating serious problems of environmental control and food safety. Production of biodiesel with waste edible oil as feedstock not only could reduce disposal problems, but, more importantly, would decrease the cost of biodiesel.

Presently industrial production of biodiesel from waste edible oil is performed by chemical alkaline catalysts, but it has been found that high content of free fatty acid (FFA) in waste edible oil (FFA>2%) would decrease the yield sharply due to soaps formed in the process[1]. Several studies showed that enzymatic methanolysis with waste edible oil was a promising alternative owing to its mild reaction condition and free of chemical waste.[2, 3] However, this conventional protocol was associated with many drawbacks such as deactivation of lipase caused by methanol and absorption of glycerol to lipase surface, thus resulting in serious negative effect on the reaction.[4, 5]

Du *et al.* have recently reported that methyl acetate was an effective acyl acceptor for biodiesel production.[6] To the best of our knowledge, the biodiesel production from waste edible oil with methyl acetate as the acyl acceptor has not yet been reported. Therefore, the transesterification of different kinds of waste edible oil to biodiesel with methyl acetate in a solvent free system was explored in this paper and the major influential factor on the reaction was further investigated.

Experimental

Materials. One waste edible oil (WDO-1) was collected from fast food restaurant, the other (WDO-2) was obtained from local restaurant waste oil pool and pretreated with activated clay. The refined corn oil (RCO) was purchased from local supermarket. Novozym 435 (lipase B from *Candida antarctica*, 164 U/g, 1unit corresponds to the amount of enzyme that produces 1 µmol methyl oleate from triolein per minute at 35 °C) was kindly donated by Novo Nordisk Co. (Denmark). Methyl palmitate, methyl stearate, methyl oleate, methyl linoleate, methyl linolenate and methyl heptadecanoate (as internal standard) were purchased from Sigma (USA). All other chemicals were also obtained commercially and of analytical grade.

Reaction. The reaction was carried out at 40 °C and 150 rpm. The reaction mixture contained 5 g waste edible oil, 6.93 g methyl acetate with the molar ratio of methyl acetate to total fatty acid being 16:3 and 246 U Novozym 435. The reaction conditions of the three-step methanolysis were the same as our previous study.[7] Samples of 5 µl were periodically withdrawn and mixed with methyl heptadecanoate for GC analysis.

Analysis. The methyl ester (ME) yield in the reaction mixture was assayed with a GC2010 gas chromatography (Shimadzu Corp., Kyoto) equipped with a HP-5 capillary column (0.53 mm × 15 m, HP, USA). The column temperature was hold at 180 °C for 1 min, raised to 186 °C at 0.8 °C /min and kept for 1 min, then upgraded to 280 °C at the rate of 20 °C /min. Nitrogen was used as the carrier gas at 2 ml/min. Split ratio was 1:100 (v/v). The injector and the detector temperatures were set at 250 °C and 280 °C, respectively. The water content of the waste edible oil and refined corn oil were measured by Karl Fischer titration using 787 KF Titrino (Metrohm Ltd. Switerland)

Results and Discussion

The transesterification of different oil with methyl acetate was first explored (**Figure 1**). The ME yield of WDO-1 was close to that of RCO after reaction for 24 h. However, the ME yield of WDO-2 was only 77.5%, which was lower than that of WDO-1 and RCO.

To determine the reason for the differences in ME yield, some important parameters of three kinds of oil were measured and depicted in. **Table 1**. The major difference was found to be in the content of FFA. So, the effect of the FFA on the reaction was subsequently investigated by adding different amounts of oleic acid into the refined corn oil.
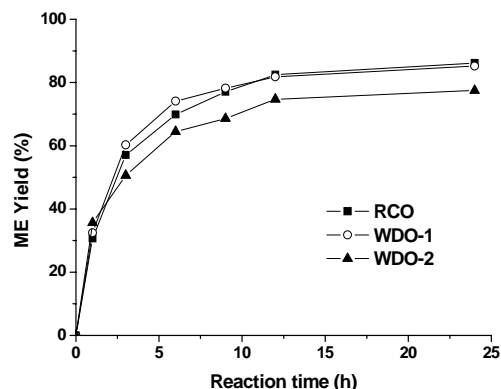

Figure 1. Time course of the reaction. The reactions were carried out at 40 °C and 150 rpm and the reaction mixture contained 5 g waste edible oil, 6.93 g methyl acetate and 246 U Novozym 435.

Table 1. Main parameters of waste edible oil and refined oil

	WDO-1	WDO-2	RCO
Water content (ppm)	320	300	250
FFA content (%)	4.6	27.8	0.1
Saponification value (mg KOH/g of sample)	193	191	187

As depicted in the **Figure 2**, the higher the FFA content, the lower the ME yield, which was similar to the result achieved in **Figure 1**, suggesting that the FFA content was the key influential factor on the reaction. However, the initial reaction rate was not significantly different, indicating that FFA showed no negative effect to the enzyme activity. Thus, acetic acid, the by-product of the process, formed in the transesterification of FFA with methyl acetate might be responsible for the decrease of the ME yield. Different amounts of acetic acid were then added directly into the RCO and the results obtained well supports the hypothesis (data not shown). This can be explained by the change of pH in the micro-environment of enzyme and thus resulted in the inhibition of enzyme activity.

To decrease the negative effect of acetic acid, some efforts have been tried by addition of different organic bases, such as tri-hydroxymethyl aminomethane (TB), triethylamine (TEA) and pyridine (PD) into the reaction mixture of WDO-2 at the beginning of the transesterification As shown in **Figure 3**, the reaction rate was markedly enhanced during the process, on the other hand, the improvement of the ME yield was also observed. Among the organic bases studied, TB was found to be the best for the reaction.
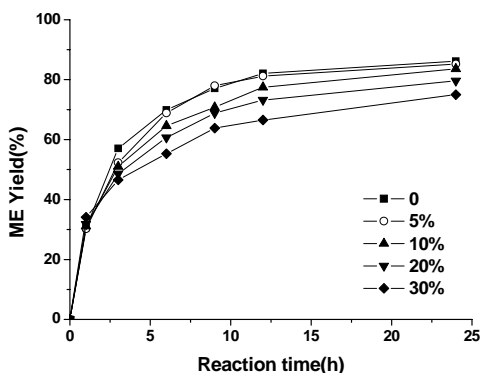
Figure 2. Effect of free fatty acid on the reaction. The reactions were carried out at 40 °C and 150 rpm and the reaction mixture contained 5 g mixture of RCO and oleic acid, 6.93 g methyl acetate and 246 U Novozym 435.
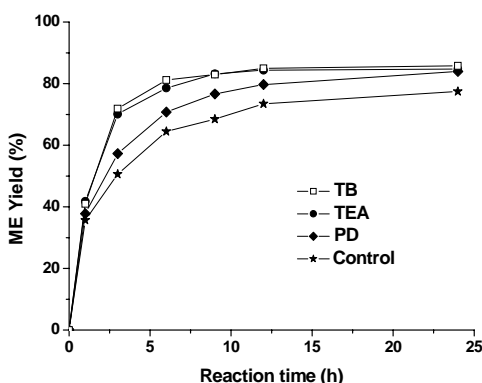

Figure 3. Effect of organic base on the reaction. The reactions were carried out at 40 °C and 150 rpm and the reaction mixture contained 5 g WDO-2, 6.93 g methyl acetate, 246 U Novozym 435 and 0.25 g different organic base.

A comparative study of biodiesel production with WDO-2 using three-step methanolysis and one-step transesterification with methyl acetate was also conducted here. The ME yield of the three-step after reaction for 72 h was 69.1%, which was much lower than those of the one-step with or without addition of organic base depicted in **Figure 3**, suggesting that the enzymatic transesterification with methyl acetate was more effective than the enzymatic methanolysis for biodiesel production.

Conclusion

The enzymatic transesterification with methyl acetate was an efficient alternative for the conversion of waste edible oil to corresponding methyl esters. The reaction rate and the ME yield were both effectively improved by addition of organic base to the reaction system.

References

(1) Ramadhas, A. S.; Jayaraj, S.; Muraleedharan, C. *Fuel*, **2005**, *84* (4), 335-340
(2) Wu, H.; Zong, M. H; Luo, Q.; Wu, H. C. *Prepr. Pap. - Am. Chem. Soc., Div. Fuel Chem.,* **2003**, *48* (2), 533-534
(3) Watanabe, Y.; Shimada, Y.; Sugihara, A.; Tominaga, Y. *J. Am. Oil Chem. Soc.*, **2001**, *78* (7), 703-707
(4) Shimada, Y.; Watanabe, Y.; Samukawa, T.; Sugihara, A.; Noda, H.; Fukuda, H.; Tominaga, Y. *J. Am. Oil Chem. Soc.*, **1999**, *76* (7), 789-792
(5) Dossat, V.; Combes, D.; Marty, A. *Enzyme Microb. Technol.* **1999**, *25* (3-4), 194–200
(6) Xu, Y. Y.; Du, W.; Liu, D. H.; Zeng, J. *Biotechnol. Lett.* **2003**, *25* (15), 1239-1241
(7) Wu, H.; Zong, M. H.; Lou, W. Y. *Chin. J. Catal.*, **2004**, *25* (11), 903-908